SURFACE QUALIFICATION TOOLPATH OPTIMIZATION FOR HYBRID MANUFACTURING

A Dissertation
Presented to
The Academic Faculty

by

Austen Thien

In Partial Fulfillment
of the Requirements for the Degree
Master of Science in the
School of Mechanical Engineering

Georgia Institute of Technology
August 2020

SURFACE QUALIFICATION TOOLPATH OPTIMIZATION FOR HYBRID MANUFACTURING

Approved by:

Dr. Christopher Saldana, Advisor
School of Mechanical Engineering
Georgia Institute of Technology

Dr. Thomas Kurfess
School of Mechanical Engineering
Georgia Institute of Technology

Dr. Katherine Fu
School of Mechanical Engineering
Georgia Institute of Technology

Date Approved: July 20th, 2020

ACKNOWLEDGEMENTS

I would like to thank my thesis advisors Dr. Christopher Saldana and Dr. Thomas Kurfess for their support, guidance, and advice throughout the completion of this thesis. I would also like to thank Dr. Saldana, Dr. Kurfess and Dr. Fu for their time and for agreeing to be on my committee and the Department of Energy for providing the research funding necessary for me to complete this thesis. Additionally, I would like to thank Tom Feldhausen for his knowledge and experience in operating hybrid machine tools and Oak Ridge National Laboratory for providing me the chance to conduct research there. I would like to thank the students and faculty of the PMRC and the EPICS Fellowship for help and support. Lastly, I would like to thank my family for encouragement and support.

TABLE OF CONTENTS

LIST OF TABLES

LIST OF FIGURES

LIST OF SYMBOLS AND ABBREVIATIONS

AM	Additive Manufacturing
SM	Subtractive Manufacturing
DED	Directed Energy Deposition
IoT	Internet of Things
MQTT	Message Queued Telemetry Transport
XML	Extensible Markup Language
JSON	JavaScript Object Notation
LAN	Local Area Network
EC2	Elastic Compute Cloud
AWS	Amazon Web Services
HTTP	Hypertext Transfer Protocol

SUMMARY

Hybrid manufacturing machine tools have been shown to have great potential in revolutionizing the manufacturing of components by combining both additive manufacturing (AM) and subtractive manufacturing (SM) processes on the same machine tool. However, a prominent issue that can occur when going from AM to SM is that the toolpath for the SM process does not take into account the geometric discrepancies caused by the previous AM step. Thus, the toolpaths used for the SM process are inefficient and can lead to increased production times and increased tool wear, particularly in the case of wire-based directed energy deposition (DED). This work discusses a methodology for approximating the geometric surface of parts manufactured using an on-machine touch probe to gather geometric data and create a digital twin of the part surface. Three different geometric approximation methods using minimal probe points are formed: triangular, trapezoidal, and an augmented hybrid of the two. Optimized SM toolpaths are created using each geometric approximation with multiple objectives of reducing total machining time, surface roughness, and cutting force. Different prioritization scenarios of the multi-objective optimization goals are evaluated to determine efficiency and quality trade-offs. Based on multi-objective optimization results for all prioritization scenarios and a comparison of the toolpaths generated for each geometric approximation, the optimal geometric surface approximation is determined to be the augmented geometric approximation. Furthermore, it is shown that prioritization of the machining time and cutting force optimization goals leads to poor performance improvements in the other optimization goals.

INTRODUCTION

1.1 Motivation

While additive manufacturing (AM) has demonstrated its potential to be a disruptive technology it still suffers from many drawbacks, like its inability to create functional part surfaces, low dimensional accuracy, and defects from the deposition process. To counter these disadvantages, modern subtractive manufacturing (SM) machine tools are incorporating AM technology to create hybrid machine tools. These machine tools have the ability to deposit material and remove material to manufacture a part with the production speed and material efficiency of AM and the dimensional accuracy of SM. Of the many deposition processes available, a popular one is wire-based directed energy deposition (DED). This process uses a focused heat source to melt inexpensive welding wire and deposit it onto a substrate. However, this process can also have unpredictable results that can cause defects and irregular part surfaces which can in turn adversely affect the SM process.

The current method of generating SM toolpaths generated for hybrid manufactured parts do not take into account the geometric discrepancies that can arise from deposition. Since parts manufactured by hybrid manufacturing machine tools may need to undergo multiple AM and SM process steps, these pitfalls can be multiplied. The surface qualification facing operation used to prepare an as-built wire DED part surface for the next deposition process step is an ideal scenario in which subtractive manufacturing toolpath optimization would be beneficial. Current methods of SM toolpath optimization are not well suited to this task as they only consider relatively flat part surfaces when

optimizing a facing operation toolpath and not the irregular surface geometry found in wire-based DED parts.

The irregular geometric surfaces caused by wire-based DED pose substantial challenges and provide singular opportunities for multi-objective optimization of subtractive manufacturing toolpaths. The gains provided from such optimization are especially applicable in the context of a hybrid machine tool where additive and subtractive manufacturing capabilities exist on the same machine. To achieve an effective toolpath optimization, it is obviously desirable to incorporate as much information as possible about the part surface's geometry. A common method of determining the geometry of part features is to use an on-machine touch probe to probe the part's surface as it is an efficient use of existing equipment and most modern machine tools already have one. An added benefit of using these on-machine probes is that modern machine tool controllers come equipped with "smart" tool capabilities that allow probe data to read from the controller and transmitted to the user and incorporated into a digital representation of the part.

One drawback to the probing method is that there is an inherent process time problem since using more probe points to gather information about the part surface inevitably results in unacceptable increases in process time. This effect is compounded when considering the fact that the surface qualification of the part may need to happen multiple times throughout the part's build. Therefore, it is desirable to approximate the surface of wire-based DED components using geometries that require a low number of probe points per deposited bead of material.

1.2 Problem Statement

Currently, there is a knowledge gap in applying SM toolpath optimization to facing of irregular part surfaces as well as a method of efficiently gathering enough geometric data about the part's surface so that a proper toolpath optimization can be effected. The purpose of this work is to examine different geometric approximations of a wire-based DED part surface that use minimal probe points and to then use those geometric approximations as the basis for a multi-objective optimization of the surface qualification facing operation. The optimization results for the different geometric surface approximations must be evaluated to determine if there is an optimal geometric surface approximation. To further determine the effectiveness of this geometric approximation methodology, different optimization objectives must be prioritized and the optimization results evaluated.

1.3 Thesis Organization

The remainder of this thesis document is organized in the following manner: Chapter 2 provides background and describes the optimization problem in more detail. Chapter 3 is a literature review of the applicable fields of study to this work. Chapter 4 outlines the experimental methods used to conduct this research. Chapter 5 details the results of the study and provides a discussion about them. Chapter 6 lists the conclusions of the study, original contributions, and future areas of work.

BACKGROUND

2.1 Hybrid Manufacturing

Hybrid manufacturing machine tools incorporate both AM and SM processes in a single machine to maximize the benefits of the individual manufacturing processes while minimizing limitations of those processes. AM can form a part's near net shape while SM can be used to bring the part into specified dimensional tolerance and create a functional part surface. The hybrid process is shown in Figure 1 below:

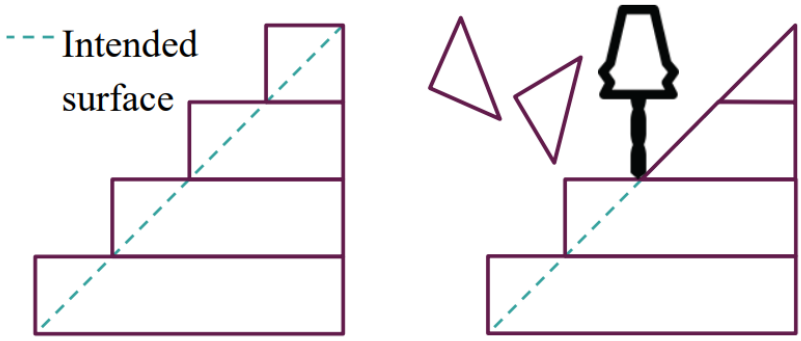

Figure 1: Hybrid Manufacturing Process [1]

In Figure 1, the rough surface of the deposited part's near net shape is cut to a smooth surface finish that is within dimensional tolerances of the intended surface. Another advantage of combing processes on the same machine tool is to mitigate part re-fixturing. Hybrid machine tools are also ideal for rework operations for high value components like molds and turbine blades [2, 3]. AM processes mostly use either powder or wire-based feedstock. Powder feedstock processes can achieve fine dimensions but the powder material is expensive, working with powder is unfamiliar to most machine shops, and the

process can only achieve low rates of deposition (5 – 30 g/min). Wire feedstock processes have less precise dimensional capability, but the wire is cheap as it is just standard welding wire, the wire process is more familiar to machine shops who have used welding processes before, and it can be used to achieve relatively high rates of deposition (up to 10 kg/h) [4]. The actual construction of hybrid machine tools typically involves attaching a deposition head to the side of the spindle in a machine tool, as seen below in Figure 2. To fully realize the production capabilities of a hybrid machine tool, it is ideal to use a 5-axis machine [5]. However, even with the maneuvering capabilities of a 5-axis machine tool, there are still geometric limitations when it comes to tool reach.

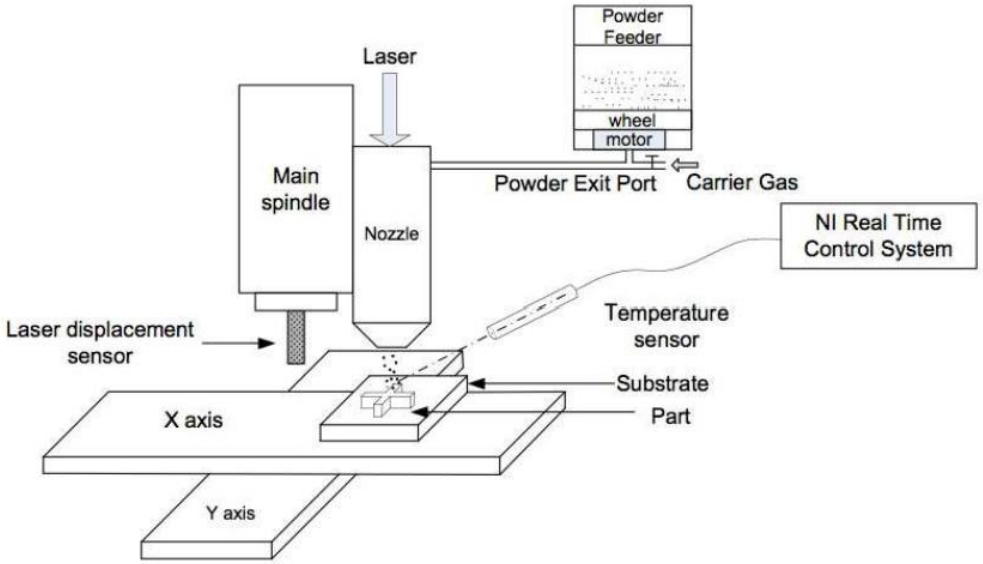

Figure 2: Hybrid Machine Tool Diagram [5]

2.2 Sectional Manufacturing Approach

Only some parts can be manufactured by depositing the full part and the machining the full part, as the length of the tools used in SM processes are limited. Furthermore, there

is also a need for a functional surface to be created on both the part's inside and outside surface, so the tool used in the SM process must have access to the part's entire surface area. These tool reach issues necessitate that parts be manufactured in sections. A diagram illustrating the sectional manufacturing approach can be seen in Figure 3 below:

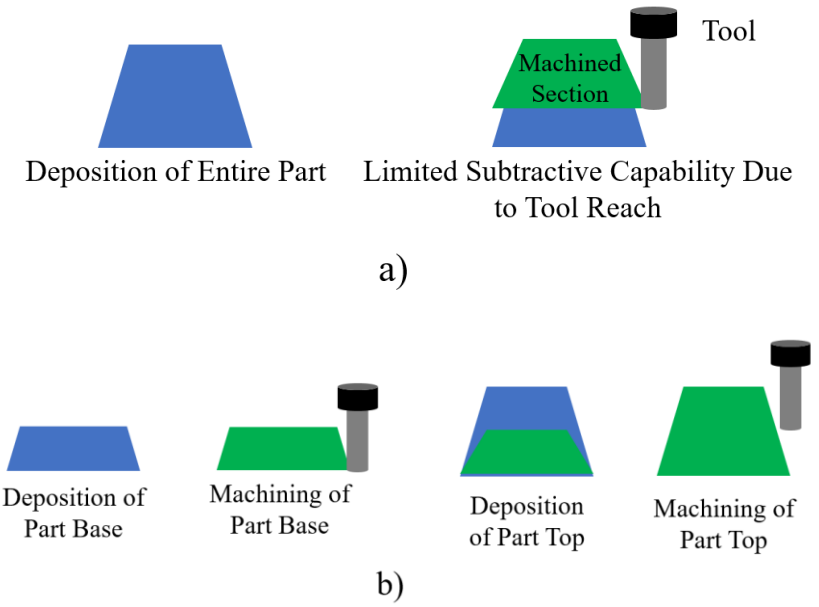

Figure 3: a) Non-Sectional, b) Sectional Manufacturing Approaches

In Figure 3a, the entire part is first deposited. However, the tool is not long enough to reach the bottom of the part so only one portion of the part can be machined. In Figure 3b, this issue is remedied by depositing and then machining the part in sections so that the tool reach never becomes an issue. Despite this improvement, there are still significant path planning challenges that occur when switching from the AM to the SM operation, since the AM process can cause geometric defects in the deposited material. Therefore, it is desirable to gather geometric data about the deposition and incorporate that into the path planning of the subtractive operation.

2.3 Toolpath Generation

The current method of generating toolpaths for hybrid manufacturing processes is to generate the AM and SM toolpaths prior to the start of any manufacturing process. Figure 4 shows this approach, wherein the desired part (in blue) is deconstructed into separate deposition and machining toolpaths (pink and brown, respectively). This approach does not take into account any of the possible geometric defects that can occur during the AM stage. The hybrid manufacturing cycle can produce geometric defects at each stage of the manufacturing process, as shown in Figure 5 below:

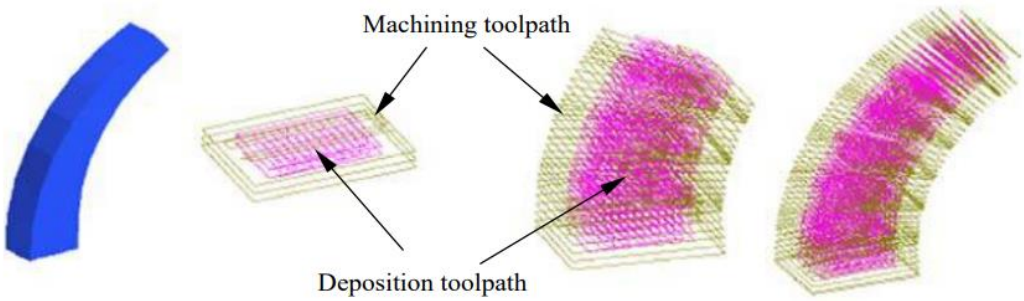

Figure 4: Current Method of Hybrid Manufacturing Toolpath Generation [6]

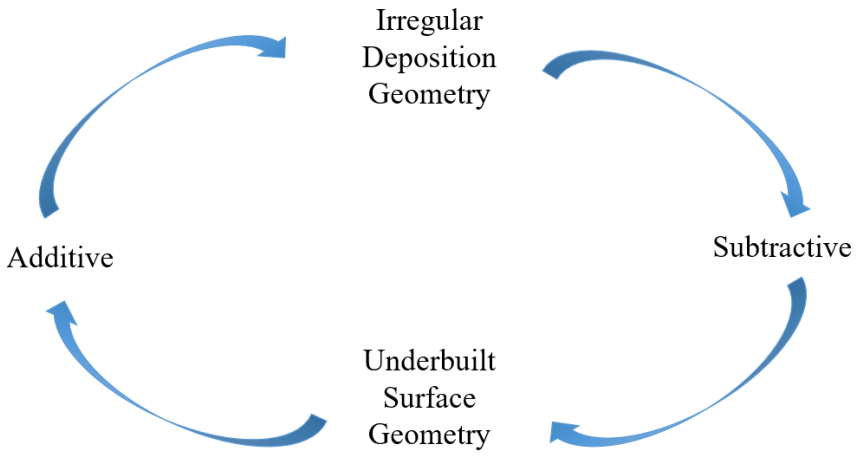

Figure 5: Hybrid Manufacturing Cycle

Figure 5 shows that the AM process can produce irregular deposition geometry and that the subtractive process can produce underbuilt surface geometries, where the geometric defects of the AM process cause the subsequent SM process to fail to remove some material. While the underbuilt surface geometries of the SM process are certainly worth investigating, the focus of this work is on the geometric defects caused by the AM process.

2.4 Deposition Geometry Issues

As mentioned previously, there can be a myriad of geometric defects that arise from the AM deposition process. These defects can be due to endemic effects of the AM deposition process or due to improper calibration of the machine tool. In this work, only several process defects that are particularly relevant to wire-based DED are discussed. The correct alignment of the melt pool created by the machine and the feeder mechanism that feeds the wire feedstock into the melt pool for deposition is crucial to ensure that all of the wire material gets deposited.

Figure 6: a) Melt Pool Feedstock Misalignment, b) Resulting Build

As seen above in Figure 6a, which is a top view of the melt pool-wire feeder interface, when the melt pool and wire trajectory do not line up much of the wire does not get properly deposited onto the part being built. This results in a part geometry that is missing material, as seen in Figure 6b, where the unmelted wire shoots off of the deposited part and leads to an overall sagging effect. Another prominent issue that can occur is illustrated by Figure 7, where the introduction of a small initial defect in the first few layers of a build can become a large defect after many layers are added.

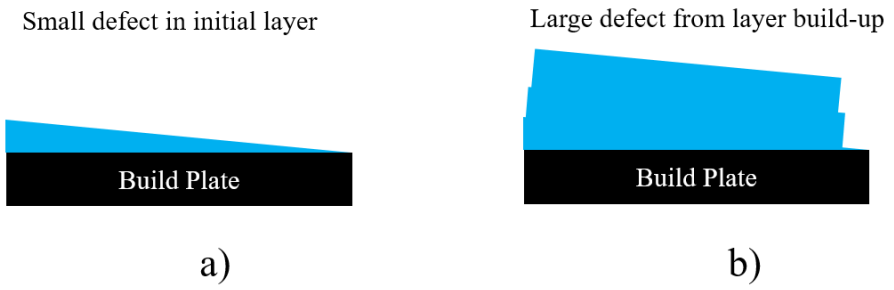

Figure 7: a) Small Initial Defect, b) Larger Built Up Defect

All AM deposition processes have issues with warping due to the thermal stresses involved in the deposition process. This can cause deposited geometries to warp out of dimensional tolerance, thereby impacting the SM toolpath. Figure 8 below illustrates the instance of a part that has warped considerably due to the thermal stresses involved in the deposition process.

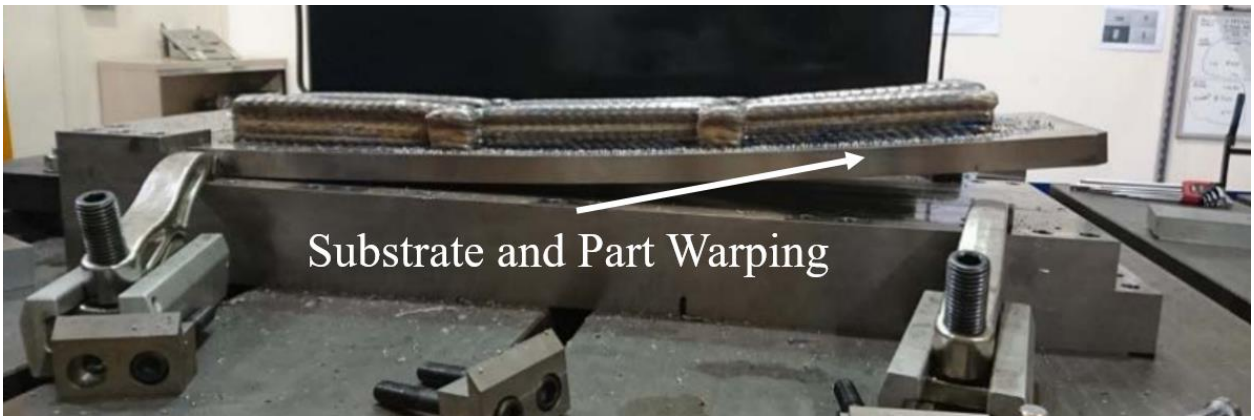

Figure 8: Part Warped from Wire DED [7]

The most concerning defect that is especially detrimental in wire-based DED processes is the build-up of deposited material that occurs during the start and stop points of a deposition track, as well as when the deposition head is rounding a corner to change direction. This defect occurs due to the fact that the material deposition rate is constant through the AM process, while the traverse rate of the deposition head accelerates when starting, stopping, or rounding a corner. The practical result of this defect can be seen in the single track deposition shown in Figure 9 below.

Figure 9: Built-Up Start and Stop Points of Bead

The built-up start and stop points of the bead are seen to be much wider than the intermediate portion of the deposition track and are also thicker than the intermediate portion of the deposition track. A pronounced example of this defect on a fully-built part can be seen in Figure 10 below.

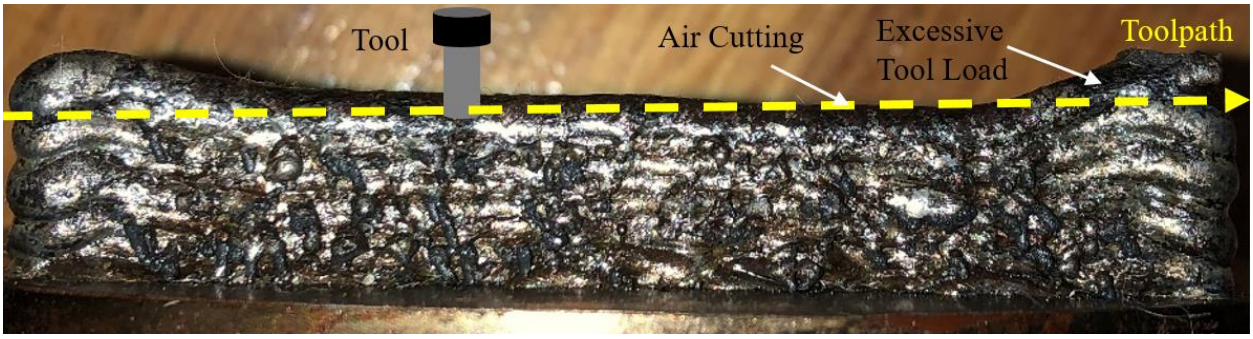

Figure 10: Air Cutting and Excessive Tool Load in Facing Toolpath for Wire DED Geometry

As described earlier, small initial defects in a deposition can cause much larger defects in the completed part shown above. The two ends of this part are significantly higher than the height of the middle portion of this part. The example SM process toolpath trajectory of Figure 10 represented by the dotted yellow line shows that there are significant machining challenges due to this distorted geometry, namely increased air cutting which adds unnecessary process time and excessive cutting tool loads that can increase tool wear or cause the tool to break. Therefore, it is desirable to determine some geometric information from the deposited part so that an optimized SM toolpath can be generated that ameliorates these issues.

2.5 Industry 4.0 and the Digital Twin

The fourth industrial revolution has mainly compromised the integration of cyber-physical systems into manufacturing environments to create the industrial internet of things (IOT). IOT is the interconnection of computing devices embedded into everyday objects that enable them to send and receive data. To create more efficient communication these IOT devices are connected using a decoupled digital architecture, meaning that the devices communicate with a well-defined interface instead of directly with each other. One of the

most common instances of this decoupled digital architecture is using MQTT, whereby a formatted message with a specific topic is sent to a server which then distributes that message to other devices. Messages are sent and received via a publish/subscribe methodology.

In a manufacturing environment this involves monitoring the manufacturing process and transmitting process data. The data can be used for a variety of things from automation to machine learning, but a significant end goal is to use the gathered process data to construct a digital twin, which is a virtual representation of a real world asset. To create the digital twin for legacy machine tools, external sensor packs are installed on components like spindle motors. For modern machine that have some smart tool capabilities, machine and process data can be read from the machine's controller and transmitted. Modern machine tools may use a number of different communication protocols to transmit data, but one widely adopted protocol for this purpose is called MTConnect and it allows one to read controller data in JSON or XML format through a LAN connected gateway or edge device. Since most hybrid machine tools are not retrofits, meaning that they have smart tool capabilities, this work describes an implementation using MTConnect to read data generated by an on-machine Renishaw touch probe.

2.6 Toolpath Optimization Problem

While it is certainly necessary to machine the entirety of the part surface, this work focuses on the narrower problem of qualifying the top surface of a part prior to the next AM process step, as illustrated in Figure 11. Qualifying the part surface means that the as-built surface, shown in Figure 11a, must be machined, or faced, down to the programmed

height, shown in Figure 11b, so that the deposition head can deposit the proper amount of material in accordance with the desired part geometry. Since this is a facing operation, only 3-axis toolpaths are considered.

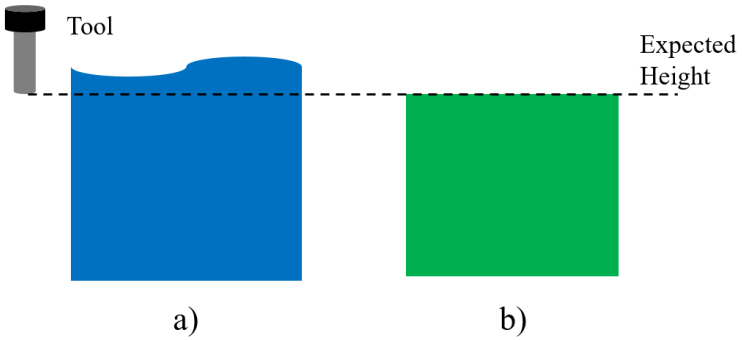

Figure 11: a) As-built surface with built-up defects, b) Faced and qualified surface

To analyze the unique optimization problem that occurs with wire-based DED part surfaces, it is best to view the part defect shown in Figure 10 as a cup-shaped geometry. This cup-shaped geometry is digitized when the individual probe points of the parts surface are connected together to form a digital twin of the part surface. An example "cup" geometry can be seen in Figure 12a with its digitized counterpart shown in Figure 12b. Note that each individual probe point is connected with a straight line, though it is shown later in this work that this may not be the case in practice.

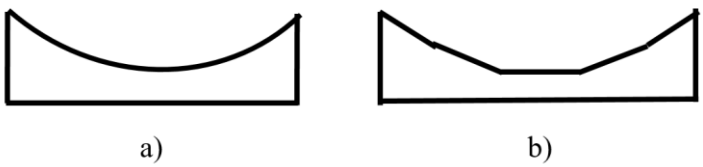

Figure 12: a) Example Cup Geometry, b) Digitized Example Cup Geometry

As mentioned previously, there are two main issues that arise due to the "cup" geometry defect. First, there is the issue of increased air cutting. Air cutting is when a

cutting tool is traversing over a part at a cutting feed rate but not actually engaging with the part. The "cup" geometry defect produces many regions where air cutting occurs, as illustrated in Figure 13 below. From the figure, the many air cutting sections needlessly increase production time since the cutting tool is moving at a cutting feed rate when it does not have to. It is therefore desirable to incorporate the geometric information gained from probing so that appropriate increases to the feed rate can be applied to the toolpath during these air cutting sections.

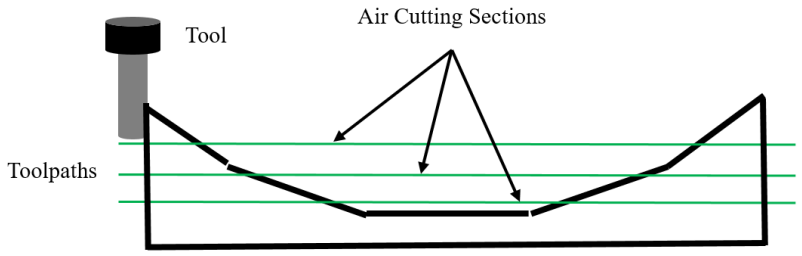

Figure 13: Air Cutting Issue from "Cup" Geometry

The other prominent issue is the irregular tool loading due to the changing slopes of the cup-shaped geometry. Figure 14a below shows that when the cutting tool engages with a section of the part geometry that has a positive slope, there is an increase in the tool's axial depth of cut which causes there to be irregular tool loading along a given toolpath. This irregular tool loading is undesirable for a number of reasons. It has been shown in multiple studies that having a constant engagement of the tool with the work piece, and therefore constant cutting force, can improve tool wear by minimizing cutting force spikes and improve machining accuracy by minimizing the variations of the tool's deflection during cutting [8, 9]. Furthermore, by minimizing the cutting force the amplitude of the vibrations from cutting is also reduced [10]. To minimize the cutting force and make

the engagement of the cutting tool more uniform, adaptive toolpaths must be created that conform to the cup-shaped geometry, as shown in Figure 14b.

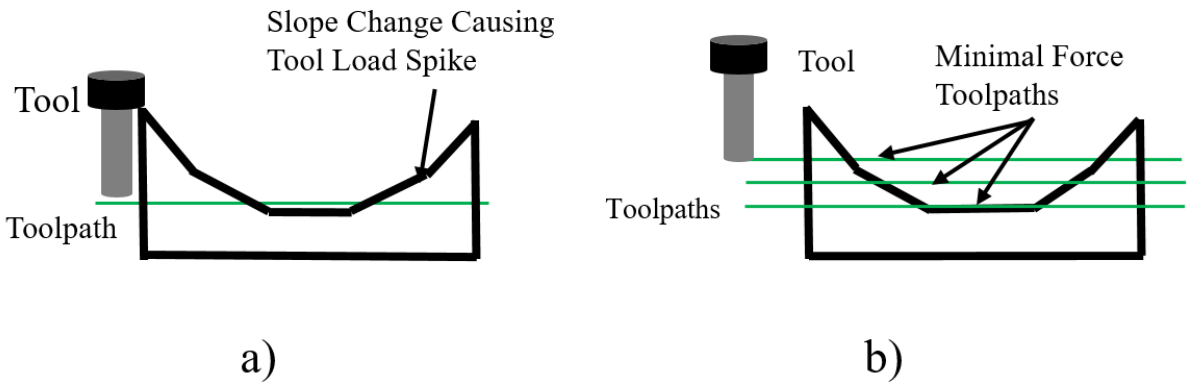

Figure 14: a) Increased Tool Load Due to Part Slope, b) Minimal Force Adaptive Toolpaths

An SM toolpath optimization methodology must be utilized to counter both of the issues previously described. This can be achieved by varying the axial depth of cut and the cutting feed rate to achieve toolpaths that minimize the cutting force and machining time, as illustrated in Figure 15 below. For each selection of an axial depth of cut and cutting feed rate for the adaptively layered toolpaths, the feed rate of the air cutting sections of each toolpath segment, shown in red in Figure 15, are increased to the rapid traverse feed rate of the machine. Lastly, in addition to minimizing the machining time and the cutting force, the surface roughness must also be minimized. This is done to avoid regenerative chatter and to achieve the desired surface finish for the part [10].

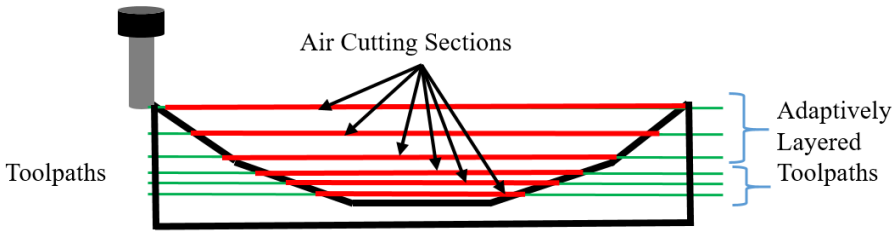

Figure 15: Optimized SM Toolpath

LITERATURE REVIEW

3.1 Wire-Based DED Process Monitoring

The previous work done in process monitoring for wire-based DED has focused primarily on process control. The weld quality of the DED process is obviously of high importance and there is a large body of work in existence focusing on monitoring the weld of the deposition to maintain quality standards. Liu et al [11] used an optical spectrometer set-up to monitor the plasma intensity to determine optimal settings for good welding. They also used a CCD camera and green laser set-up to image the melt pool to monitor the welding process's stability. This set up is shown in Figure 16 below.

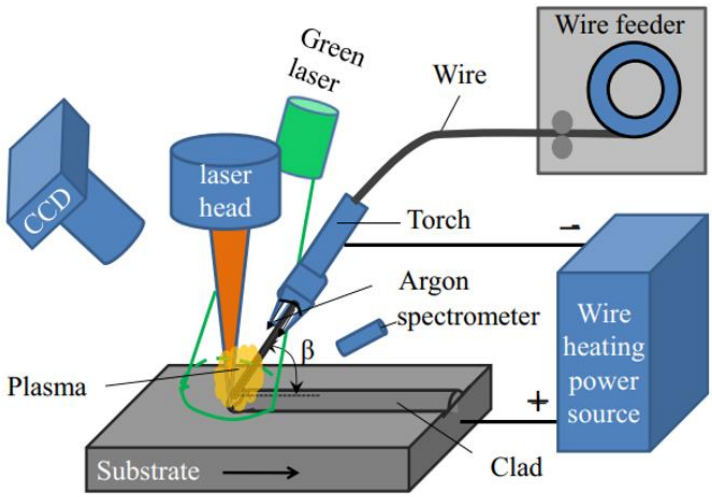

Figure 16: Clad Quality Vision Based System [11]

Heralic et al [12] used a laser line scanner set up, shown in Figure 17, to measure the deposition bead height and implemented a control algorithm to adjust layer heights in order to compensate for any disturbances found in the previous layer. However, the method

presented by Heralic et al. is geared toward use on a solely AM machine tool, not on a hybrid machine tool with SM process capability. Additionally, laser line scanners can be very expensive and produce lots of geometric data that can be lengthy and computationally expensive to process. This review serves to illustrate that there are many works regarding the monitoring and control of wire based DED processes but none on the machining of those wire based DED parts, which constitutes a knowledge gap in this field.

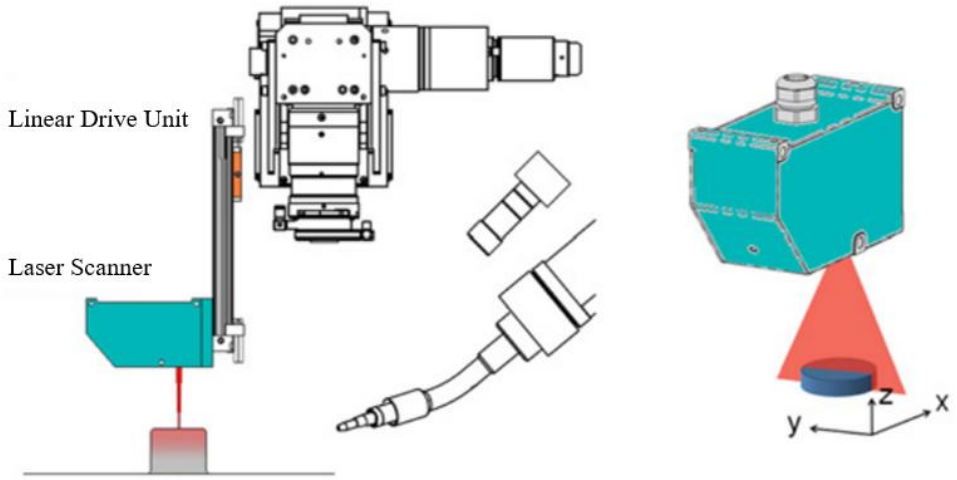

Figure 17: Laser Scanning for Layer Height Control [12]

3.2 Hybrid Manufacturing Process Data Transfer

There have been several studies that focused on the data transfer between the AM and SM stages for use in repairing turbine blades. Both Praniewicz et al. [13] and Kim et al. [14] used the on-machine Renishaw touch probe to determine the geometries of turbine blades that needed to be repaired. Praniewicz et al. used the probe data to register the unique wear that can occur in these turbine blades to form both AM and SM repair toolpaths that are adaptive to the individual needs of each turbine blade. Kim et al. used the probe data to register 2D cross-sections of the turbine blades and test different digitization strategies for

creating AM and SM repair toolpaths. Models of these two methods can be seen below in Figure 18:

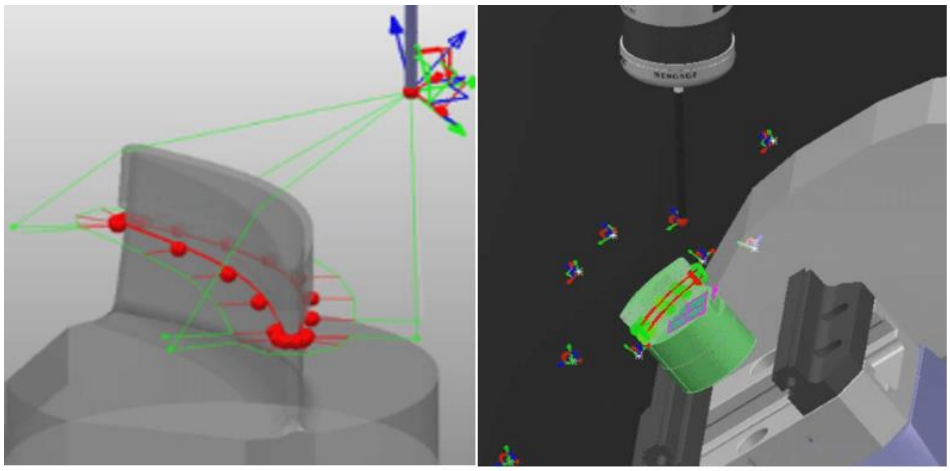

Figure 18: a) 2D Profile Probing, b) Model Registration Probing [13,14]

Both of these methods required generating complex 5-axis probing, AM, and SM toolpaths since the geometry of the turbine blades was complex and necessitated using a highly maneuverable CNC. Additionally, the probing toolpaths were generated via PowerInspect, and the probe data had to be gathered using a LAN connected laptop. This review serves to illustrate that while there are works that implement geometric data transfer from AM to SM stages via an on-machine touch probe and LAN connected laptop, those processes are limited to repair and rework operations and utilize complex 5-axis toolpaths and licensed software. Thus, there is a knowledge gap in the field when it comes to geometric data transfer using MTConnect and Industry 4.0 methods for use in generating 3-axis toolpath surface qualification facing operations via an open-source software.

3.3 Subtractive Toolpath Optimization

There is a larger body of work already available in the domain of optimizing SM toolpaths and process parameters using a variety of techniques and with a variety of goals. As such, only a handful are discussed in this work. For single objective optimizations, Castelino et al. [15] focused on minimizing the travel time between successive toolpath segments by utilizing the well understood traveling salesman problem where the start and stop points of each toolpath segment were fed into a heuristic algorithm that optimally connected the toolpath segments. Lazoglu et al. [16] studied how to find global cutting force minimal toolpaths in the ball milling of free form surfaces by testing different orientation angles of the toolpath in the XY plane and determining the toolpath with the lowest maximum cutting force. Corso et al. [17] introduced surface roughness as a constraint to the optimization focusing on minimizing machining time by varying different cutting parameters.

The SM process can also be optimized using multiple objectives that provide a more informed outlook on the trade-offs for process priorities. However, the majority of the literature this approach is focused on finding optimal process parameters without focusing on the toolpath of the process. Maiyar et al. [18] found the optimal machining parameters for end milling Inconel 718 in order to find the optimal balance between surface roughness and material removal rate and Shaik et al. [19] found optimal machining parameters for end milling Al-6061 while minimizing surface roughness and tool vibration amplitudes. An et al. [20] primarily focused on the optimal machining parameters for face milling with an eye to minimizing the unit production cost and total machining time with cutting force and surface roughness as constraints. Ali et al. [21] did focus on testing different face

milling toolpath strategies for flat part surfaces to determine how the path strategies affected surface roughness and material removal rate. From a sustainability perspective, Yan et al. [22] performed a multi-objective optimization analysis that focused on minimizing cutting energy and surface roughness while maximizing material removal rate. Lastly, though it is not regarding optimization, tool manufacturers like Sandvik Coromant suggest avoiding face milling over holes or slots since that cause multiple entries and exits per rotation of the tool [23].

Since wire-based DED is much like the casting process, an inquiry into the optimization of machining castings is desirable to see if any strategies can be applied to the hybrid manufacturing use case. While a number of studies focused on optimizing casting parameters to obtain sufficient microstructures that minimize tool wear, Gessner et al. [24] focused on using laser scanning software to optimize the alignment of the casting with respect to the machine tool such that the minimal amount of material is removed. A 5-axis hybrid machine tool with a rotary/tilt trunnion table could be used to optimally align a deposited part but the process of laser scanning an entire part is labor intensive and not feasible for high throughput production.

While the breadth of SM toolpath optimization literature is large, there is a knowledge gap when it comes to applying toolpath optimization for facing operations to the irregular geometry of a part surface produced by wire DED. However, many of the optimization goals and formulations used in literature can be applied to the unique optimization challenge discussed in this work.

EXPERIMENTAL METHODS

4.1 Process Overview

An overview of the experimental process can be seen in Figure 19 below. The first stage of the experimental methodology used in this work is to probe each bead of the deposited part to generate a height profile for each bead. Then the height profiles for each bead are consolidated into one height profile that is used for the entire thickness of the part. To generate this singular height profile, the height value for each probe location is the highest height value of all the bead's height profiles at that particular probe location.

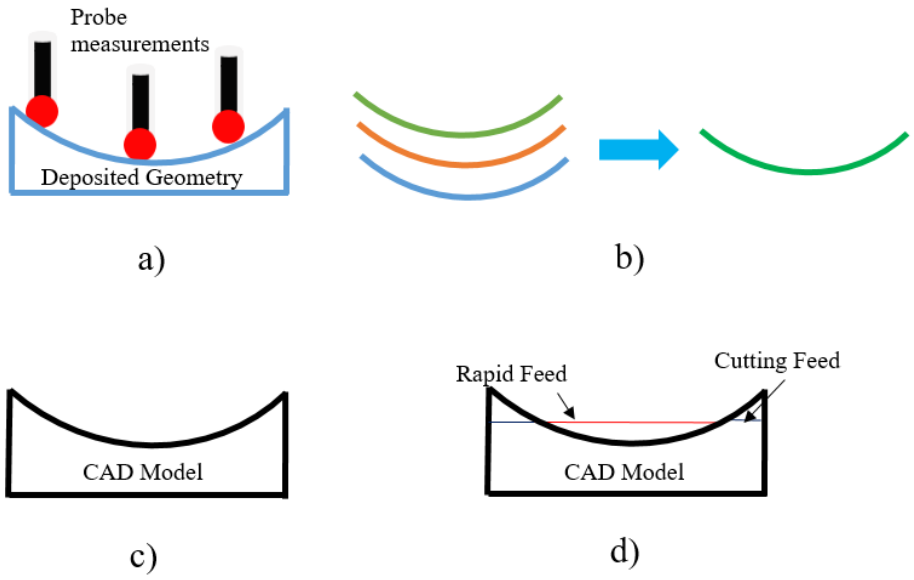

Figure 19: Experimental Process Overview: a) Probe each bead of part, b) Consolidate output from each bead into one "bead" containing highest point of all beads at each probe location, c) Create Digital Twin CAD model by connecting probe points using import spline method (Fusion360) or straight line method (MATLAB), d) Optimize subtractive toolpath using digital twin geometry

Next, a digital twin is created from the consolidated probe height profile by connecting the individual probe points. This is done with MATLAB and Fusion360. In Fusion 360, the probe points are connected using an add-in that allows XYZ data to be imported into a sketch and automatically connected using splines. The spline sketch can then be extruded out to form a 3D CAD model of the part. In MATLAB, the probe points are connected using straight lines. Once the digital twin has been constructed from the probe data, the SM toolpath is optimized.

4.2 Equipment

4.2.1 Machine Tools

The hybrid machine tool chosen to manufacture the sample part is the Mazak VC-500A/5X AM HWD recently created by Mazak Corporation. It is a five axis vertical machining center that has been augmented with a 4 kW laser and deposition head [25]. The machine tool chosen for the probing operation is the Mazak VC-500A/5X, which is purely a subtractive manufacturing machine tool [26]. Both machines use an on-machine Renishaw touch probe and feature MTConnect capable controllers. The probing operation is run on a separate machine due to logistical reasons.

4.2.2 On-Machine Touch Probe

The Renishaw touch probe used for the probing operations features its own set of G-Code instructions that can be used to program canned cycle probing operations for typical part features like bosses, webs, and bores. It is also able to perform single surface probing operations to determine work piece offsets. The command used in this work is the G65

single surface probing command. There are a variety of command parameters that can be used to determine the height profile of a part [27], such as G65P9901M1.C1.X_.Y_.Z_.A-3.K_. The most notable features of this G-Code command are the "C1" portion which allows the probe to do successive probing operations without turning off, the "X.Y." portion that denotes the start position of a probing operation and the "K." portion that denotes the expected height of the part feature being probed. After setting the work piece Z offset value as the build plate surface and substituting the expected part height into the G-Code, one can generate a series of probe commands to perform probing operations at varying points of the part surface's XY plane by plugging in XY values from the part's deposition path to achieve a desired probing resolution. This probing resolution is measured in unit length/probe point, where the unit length is the distance traveled along the part's deposition path. The probe data is then stored in macrovariable #100 on the machine controller, where it can be retrieved via the MTConnect gateway.

4.3 Digital Architecture/Geometric Data Acquisition

To expediently capture and transmit probe data, a decoupled digital architecture is implemented similar to the one described earlier in this work. An EC2 instance, which is a virtual machine run by AWS, is used as an MQTT message broker that transmits the probe data. Since the Mazak HWD comes with MTConnect capability, a low-cost Raspberry Pi 3 B+ micro-processor is used as an edge device [28]. This edge device uses an HTTP request/response to read the controller's macrovariable values via MTConnect. Then the edge device transmits the probe data wirelessly to the MQTT server by publishing it to a specific message topic. The user's device, or client, is connected to the MQTT server and is subscribed to the same topic as the edge device, and thus can receive the probe data and

store it in a local file for later use. A schematic of the digital architecture used in this work can be found in Figure 20 below.

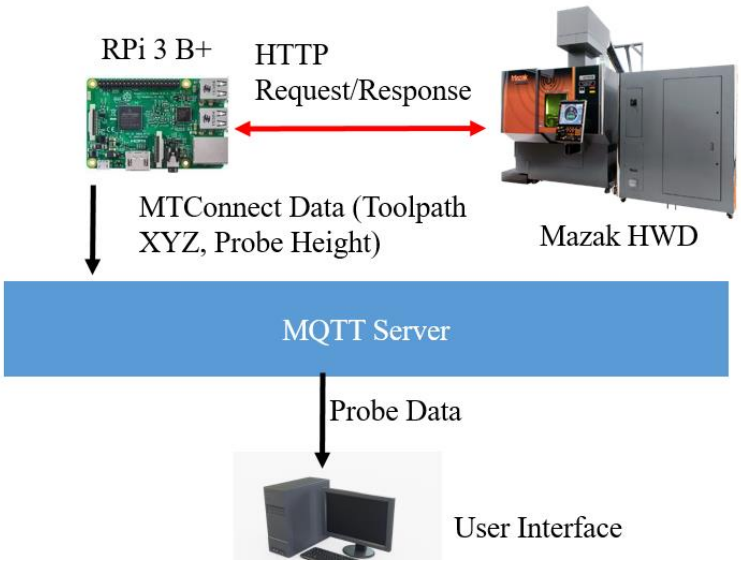

Figure 20: Digital Architecture [28, 29]

4.4 Sample Part Fabrication

To test out this experimental methodology, a sample part is fabricated using the Mazak HWD. The part is made from 316 stainless steel and has dimensions of 6.58 x 79.94 x 11.51 mm. The deposition parameters used for the part can be seen below in Table 1:

Table 1: Sample Part Deposition Parameters

Feed Rate (mm/min)	Laser Power (W)	Hot Wire Power (W)	Hot Wire Feed Rate (ipm)
1067	2250	700	175

These deposition parameters are nominal for processing 316 SS. The path planning of the part is made specially to exaggerate the cup-shaped geometry defect, and can be seen in Figure 21. Figure 21 shows a view of the XY plane of the deposition where the arrow

indicates the deposition path trajectory. Instead of using a raster pattern to deposit the three bead thick part, each bead is deposited as a single track similar to that found in Figure 9. Furthermore, the direction of the deposition path is rotated 180 degrees for each alternating layer of the part.

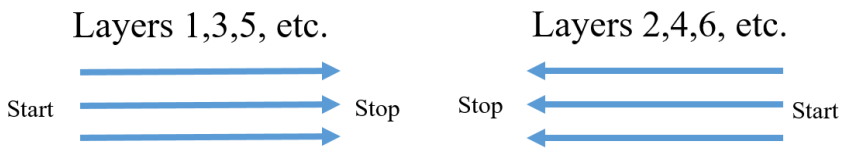

Figure 21: Sample Part Path Planning

4.5 Geometric Surface Approximations

Earlier in this work, the need for geometric approximations of the wire DED's part surface was established. Therefore, three geometric approximation profiles are considered. The first is a triangular approximation composed of three probe points per bead (one at the start and stop points of the part and one at the middle), the second is a trapezoidal approximation composed of five probe points per bead (one at the start and stop points of the part and three more that are equally spaced between the start and stop points), and the last is an augmented approximation using five probe points per bead with a lower probing resolution at the start and stop points of the part. Figure 22 below shows an example of what the part's digital twin would be like with these geometric approximations.

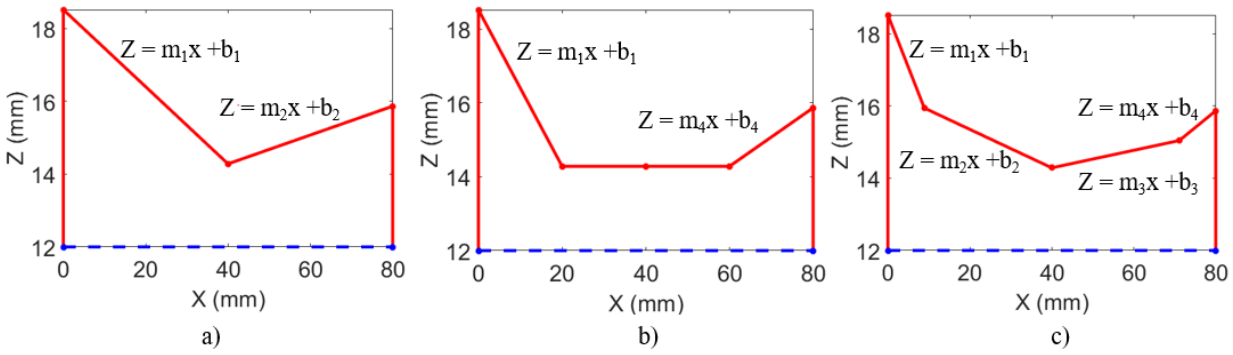

Figure 22: a) Triangular Approximation, b) Trapezoidal Approximation, b) Augmented Approximation. Height profile is shown in red, desired Z height is shown by the dotted blue line.

The height profile of the geometric approximation is shown in red. Note that the Z dimension of the part has been truncated to only show the part geometry above the desired Z height. With these geometric approximations, there are three key path geometry parameters: the path length, the difference in height of the start and stop points (also known as the corner height), and the absolute height difference between the highest and lowest points of the height profile. Note that the triangular approximation's height profile in Figure 22a just consists of two straight lines at that connect the start point to the middle point and the middle point to the stop point. The trapezoidal approximation's height profile in Figure 22b consists of four straight lines that connect the points together, but the lines that connect the three intermediate points together are all horizontal. The augmented approximation's height profile in Figure 22c consists of four straight lines that connect the points together, but the second and fourth probe points are located closer to the start and stop points. This allows the augmented approximation to better conform to the cup-shaped geometry. Using the simplified geometry of straight lines for the approximations allows for the equations of those lines to be easily found in the typical linear format.

After the part surface has been approximated, the subtractive tool path is then optimized. Each geometric approximation has different stages of the toolpath optimization in accordance with the approximation geometry. In the example optimizations shown below, the blue toolpath lines indicate toolpath sections when the tool is traveling at a cutting feed rate and the green toolpath lines indicate toolpath sections when the tool is traveling at a rapid traverse feed rate. Note that the retract moves are not shown in those figures for clarity. In all three cases, the tool is traveling from the left to right in accordance with conventional milling, and after each pass is completed it retracts to the starting X position and descends to the next toolpath level. Note that this optimization assumes that the part is being faced using a single pass of the tool for each toolpath level. Also note that these are just example optimizations used to illustrate the method.

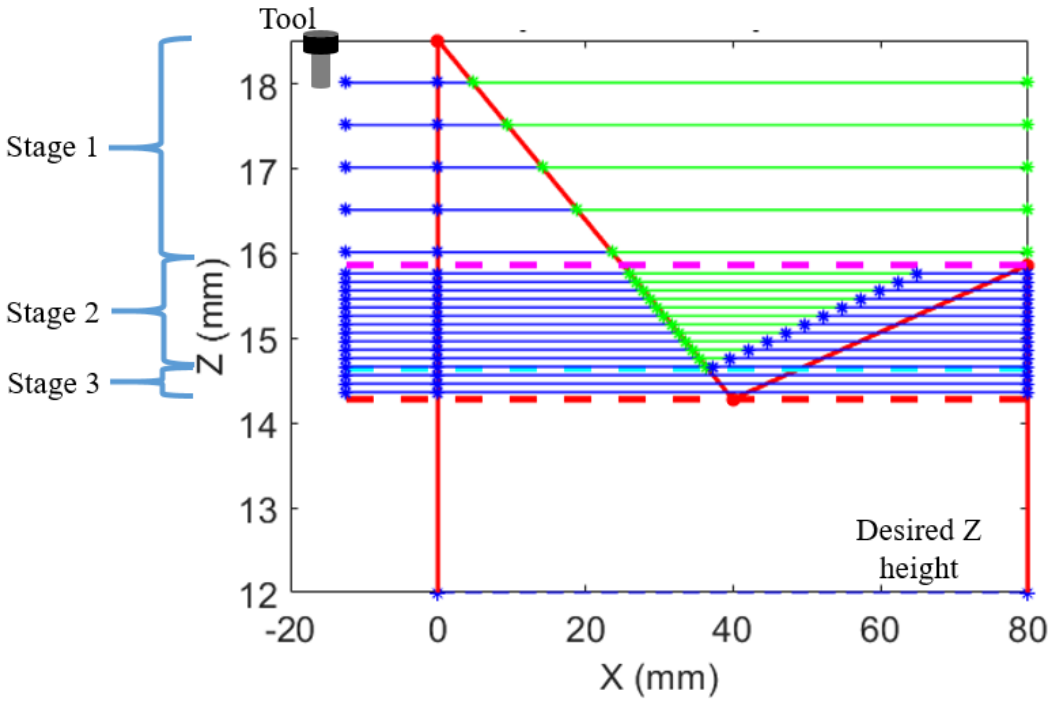

Figure 23: Example Triangular Approximation Toolpath Optimization. Height profile is shown in red, and desired Z height is shown by the dotted blue line. Stage 1 end is indicated by the dotted pink line, Stage 2 end is indicated by the dotted cyan line, and Stage 3 end is indicated by the dotted red line.

When considering the triangular geometric approximation, there are three stages of toolpath optimization as shown in Figure 23. The first stage is optimizing the machining from the high corner of the part to the low corner, and the only improvement made on this toolpath is to decrease machining time by using a rapid feed rate on the air cutting portions. The second stage is optimizing the machining from the low corner of the part until the distance between the two lines of the triangle is equal to one tool radius, as at that point the tool can no longer travel at a rapid feed rate during the air cutting sections since it crashes into the other side of the part. The third stage is just machining from the end of the second stage down to the lowest point of the triangle. The optimization for the toolpath segments in the second and third stages is focused on balancing the minimization of cutting force, machining time, and surface roughness.

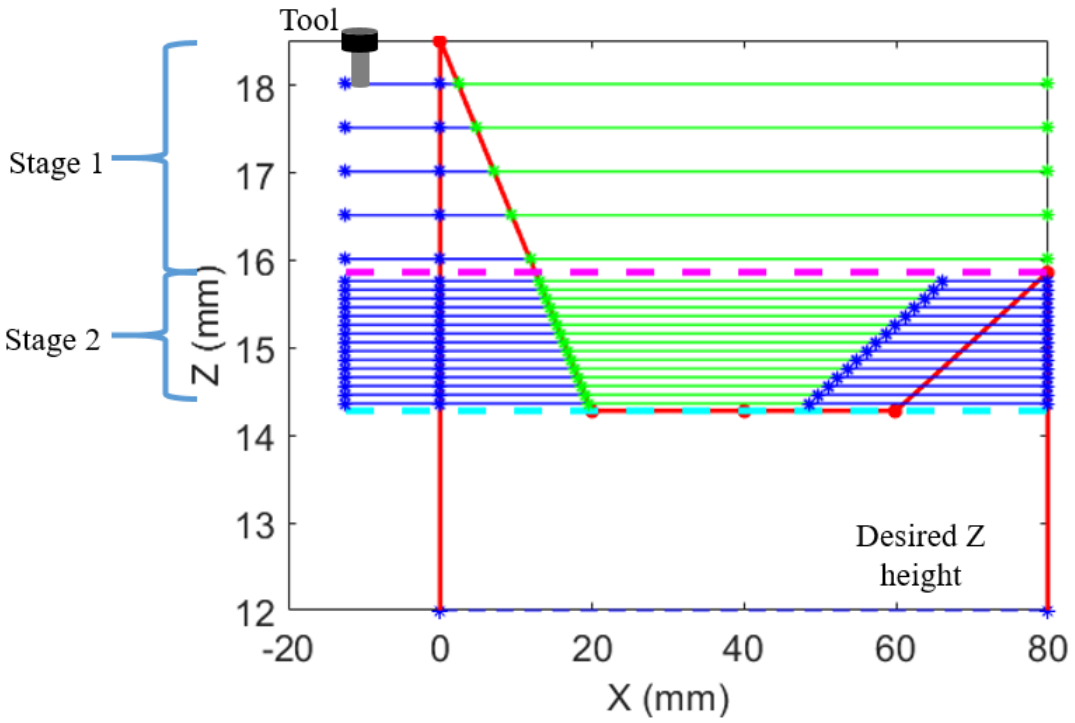

Figure 24: Example Trapezoidal Approximation Toolpath Optimization. Height profile is shown in red, and desired Z height is shown by the dotted blue line. Stage 1 end is indicated by the dotted pink line, and Stage 2 end is indicated by the dotted cyan line.

When considering the triangular geometric approximation, there are two stages of toolpath optimization as shown in Figure 24. The first stage of the trapezoidal optimization is just like the triangular one, where the part is machined from the high corner of the part to the low corner, and the only improvement made on this toolpath is to decrease machining time by using a rapid feed rate on the air cutting portions. The second stage is optimizing the machining from the low corner of the part until the base of the trapezoid is reached. As with the triangular approximation, the optimization of the toolpath segments for the second stage of the trapezoidal approximation is to balance the minimization of cutting force, machining time, and surface roughness.

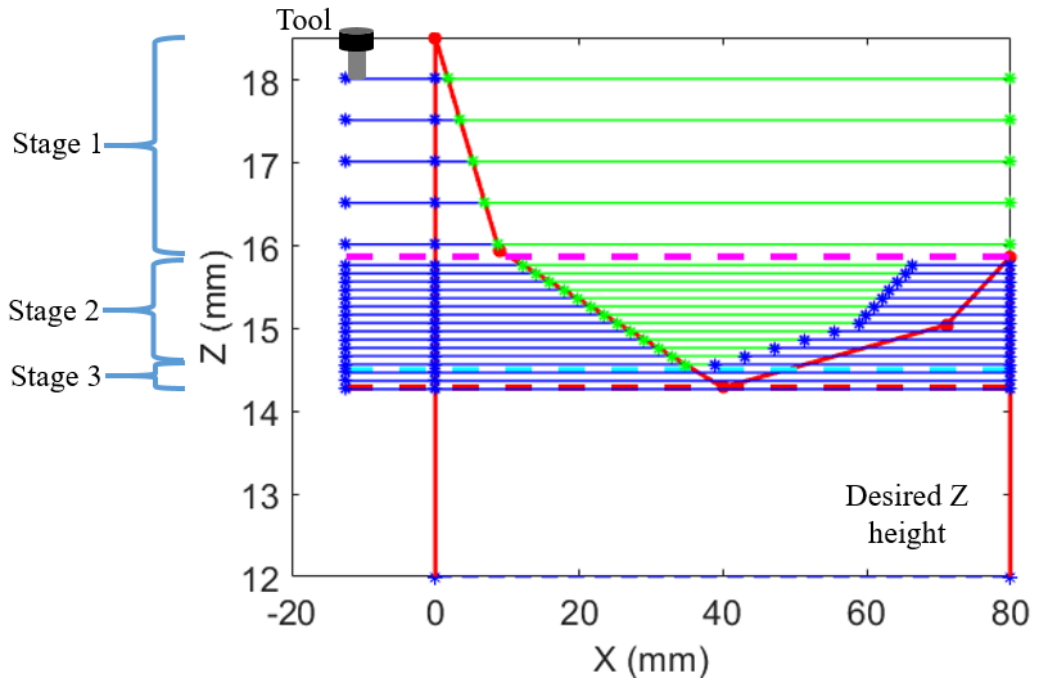

Figure 25: Example Augmented Approximation Toolpath Optimization. Height profile is shown in red, desired Z height is shown by the dotted blue line. Stage 1 end is indicated by the dotted pink line, Stage 2 end is indicated by the dotted cyan line, and Stage 3 end is indicated by the dotted red line.

When considering the augmented geometric approximation, there are three stages of toolpath optimization as shown in Figure 25 below. The first stage of the augmented optimization is just like the triangular one, where the part is machined from the high corner of the part to the low corner, and the only improvement made on this toolpath is to decrease machining time by using a rapid feed rate on the air cutting portions. The second stage is just like the triangular approximation where the toolpath is optimized from the low corner of the part until the distance between the second and third lines is equal to one tool radius, as at that point the tool can no longer travel at a rapid feed rate during the air cutting sections since it crashes into the other side of the part. The third stage is again like the triangular approximation, where the part is machined from the end of the second stage down to the lowest point of the height profile. The optimization for the toolpath segments in the second

and third stages is focused on balancing the minimization of cutting force, machining time, and surface roughness.

4.6 Toolpath Optimization Formulations

The formulation of the SM toolpath optimization problem is composed of varying input parameters that are subject to a variety of different constraints. The input parameters discussed earlier in this work are the axial depth of cut, or Adaptive Layer Thickness (mm), and the Adaptive Feed Rate (mm/min). The constraints for these input parameters are given below:

$$0 < d_o < StepDown \quad (1)$$

$$0 < f_o < f_{max} \quad (2)$$

Where d_o is the Adaptive Layer Thickness, StepDown is the axial depth of cut used in the non-optimized cutting condition, f_o is the Adaptive Feed Rate, and f_{max} is maximum available cutting feed rate on the machine tool. There are also additional constraints put on the optimization goal values of machining time and cutting force. To have viable optimized toolpaths when compared to the non-optimized toolpaths it is desirable for the optimized machining time value to be less than or equal to the non-optimized machining time value. If the optimized machining time value were greater than the non-optimized machining time value, than the added process time of the probing operation would make the optimized solution undesirable. Likewise, if the optimized cutting force is greater than the non-optimized cutting force, there would be worse tool performance so that optimized solution is also desirable.

The optimization goals for each set of input parameters must be calculated from the input parameters, and the equations for those goals can be seen below. The calculation for machining time is simply computed by adding up the machining times for each stage depending on the geometric approximation being used:

$$T_{total} = \sum_{1}^{n} T_n \tag{3}$$

Where T_{total} is the total machining time and T_n is the machining time for stage n. For the cutting force, a simple analytical equation can be found by equating the two definitions of cutting power [30, 31]:

$$P = F_c * V \tag{4}$$

$$V = \pi * D * N \tag{5}$$

$$P = u * MRR \tag{6}$$

$$MRR = r * d * f \tag{7}$$

By setting equations (4) and (5) equal to each other and solving for cutting force F_c:

$$F_c = \frac{u * r * d_o * f_o}{\pi * D * N} \tag{8}$$

Where P is the cutting power, V is the surface speed, D is the tool diameter, N is the RPM, u is the material's Brinell Hardness Number, MRR is the material removal rate and r is the radial depth of cut. For standardization purposes, the tool used in every optimization

scenario is a 4-flute end mill with 1-inch diameter kept at a constant 859 RPM. It should also be noted that a constant radial depth of cut is assumed, so only the d_o and f_o parameters are being changed in this optimization so it useful for the scope of this work to represent the cutting force as being proportional to the product of the two input parameters.

$$F_c \; \alpha \; d_o * f_o \tag{9}$$

The average surface roughness of the part is likewise calculated using an analytical equation:

$$Ra \; = \; \frac{s_{z,o}}{4 * \left(tan(K) + \; cot(K')\right)} \tag{10}$$

$$s_{z,o} \; = \frac{f_o}{N * Nt} \tag{11}$$

Where $s_{z,o}$ is the feed per tooth, K is the lead angle of the tool, and Nt is the number of teeth of flutes of the tool. To make the analytical solution more applicable to a variety of cutting tools, it is more useful to represent the surface roughness as being proportional to the $s_{z,o}$:

$$R_a \; \alpha \; \frac{f_o}{4 * (N * Nt)} \tag{12}$$

These expressions for the different optimization goals are then normalized based on the highest goal value from the various iterations of the input parameters and put into an objective function. The objective function is an expression that is a weighted sum of the normalized optimization goals. This formulation is useful as different prioritizations of the

optimization goals in the objective function can be achieved by changing the weight values. The weight values must also add up to 1, which is an Archimedean formulation of the objective function [32]. The objective function can be seen below, along with the Archimedean weights constraint:

$$ObjFun = W_T * \left(\frac{T_{Total}(d_o,\, f_o)}{T_{Total,max}}\right) + W_R * \left(\frac{R_a(f_o)}{R_{a,max}}\right) + W_F * \left(\frac{F(d_o,\, f_o)}{F_{max}}\right) \quad (13)$$

$$W_T + W_R + W_F = 1 \quad (14)$$

RESULTS AND DISCUSSION

5.1 Manufactured Sample Part

Using the optimal deposition parameters described earlier, a wire-based DED part is manufactured that is used as a sample for this work and is shown below in Figure 26. The part produced by the Mazak HWD has visible signs of the cup-shaped geometry defect as seen by the areas circled in green. For scale, a 1" gauge block is put onto the part.

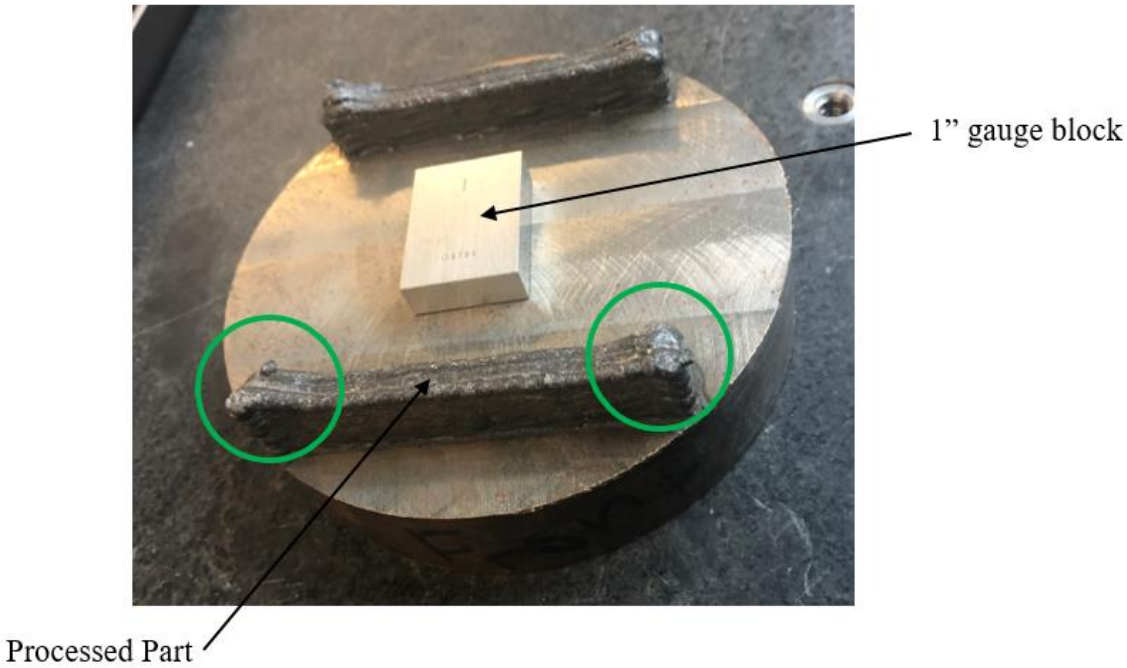

Figure 26: As-Built Wire DED Part

5.2 Probing Operation Results

Three different probing operations are performed on the part: a three-point, a five-point, and a ten-point per bead probing cycle, as seen below in Figure 27. As seen in the figure, the probing toolpaths generated probe each bead of the part using increasing number of

probe points. The more probe points used in the probing the more information about the part surface is found, however, this comes at the cost of increasing process time.

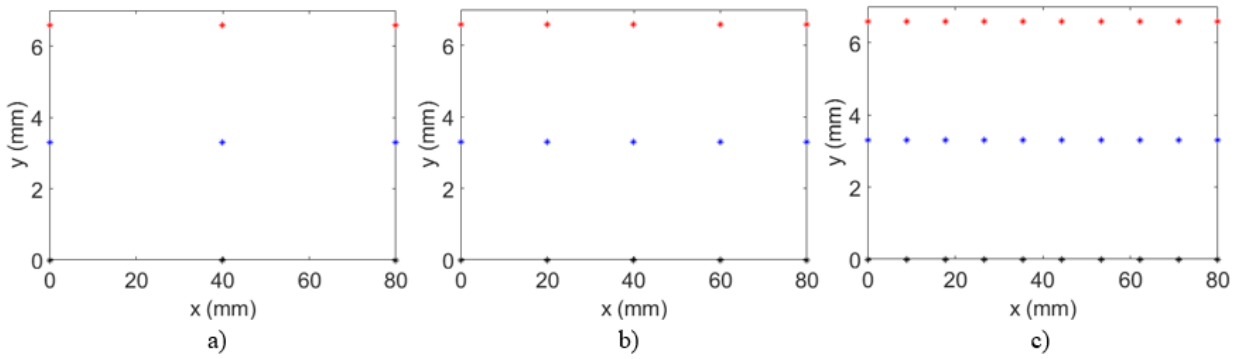

Figure 27: a) 3pt Probing Toolpath, b) 5pt Probing Toolpath, c) 10pt Probing Toolpath

The data from the three and five-point probing cycles are used to construct the triangular and trapezoidal approximations, whereas the data from the ten-point probing cycle are used to form the augmented approximation and as a higher fidelity digital twin to evaluate the different geometric approximations. Since the probing operation generates a point cloud of XYZ data, it is useful to visualize that data in MATLAB by using an interpolated 3D surface. To better understand the development of the part surface's height profile, the XZ plane of the 3D interpolated surface is shown in Figure 28 below.

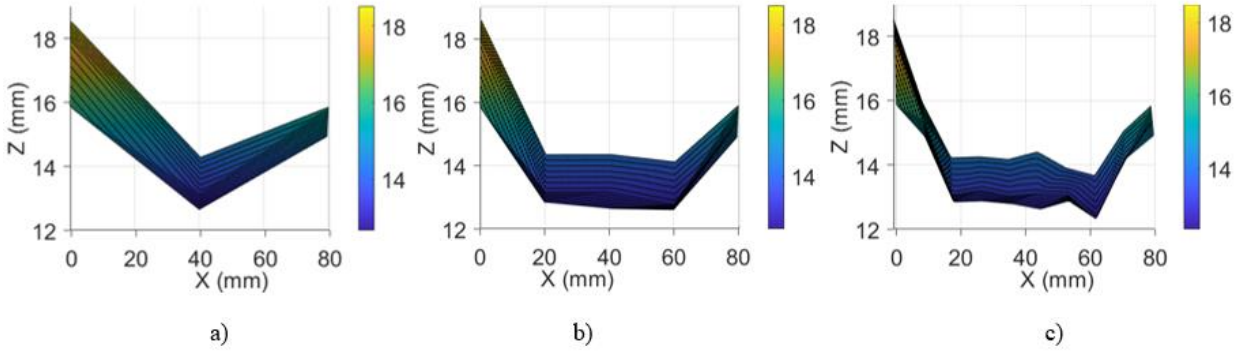

Figure 28: a) 3pt Probe Interpolated Surface, b) 5pt Probe Interpolated Surface, c) 10pt Probe Interpolated Surface

It can be seen that as more probe points are added the height profile of the part changes from a "V" shape in Figure 28a to a more trapezoidal shape in Figure 28c. However, to simplify the analysis the probe data from the height profiles of all three beads are consolidated into a single height profile, as shown below in Figure 29:

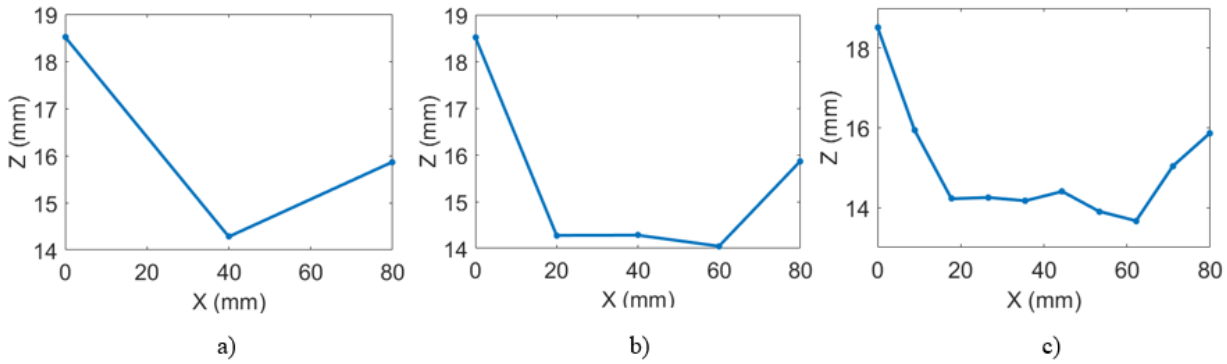

Figure 29: a) 3pt Consolidated Height Profile, b) 5pt Consolidated Height Profile, c) 10pt Consolidated Height Profile

The consolidated height profiles validate the choices of the triangular and trapezoidal geometric approximations as those conform to the 3pt and 5pt consolidated height profiles shown in Figure 29a and Figure 29b, respectively. It is also worth noting that the higher fidelity 10pt consolidated height profile in Figure 29c shows that the increases in height

due to the cup-shaped geometry defect occur fairly close to the start and stop points of the part. This further validates the choice of the augmented geometric approximation which has a higher concentration of probe points at the start and stop of the part.

5.3 Digital Twin Construction

Once the probe data has been consolidated into a single height profile, it must then be converted into a digital twin. Using the import spline add-in of the CAD/CAM software Fusion360, the consolidated height profile can be exported in as a sketch and each point is then connected with a spline curve. This development of the height profile with this method is similar to that of the MATLAB consolidated height profile development, as shown below in Figure 30:

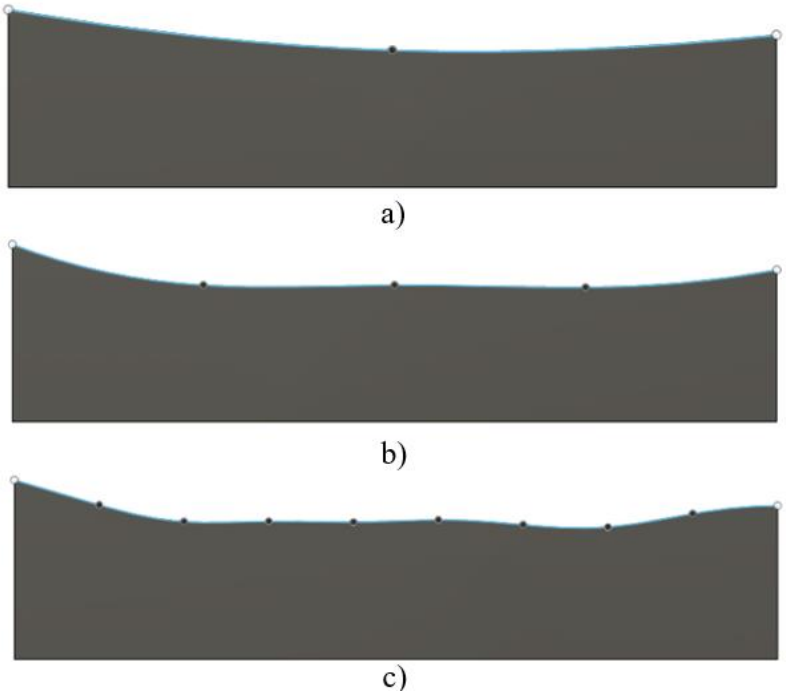

Figure 30: a) 3pt Import Spline, b) 5pt Import Spline, c) 10pt Import Spline

As seen in Figure 30 above, the height profile changes in a similar qualitative manner to that of the MATLAB results in Figure 29. However, the import spline method uses spline curves to connect the points instead of straight lines. While Fusion360 is not able to perform the subtractive toolpath optimization it useful to know if the import spline method can be used a valid approximation to the straight line method since the import spline add-in automatically creates the sketch. By creating another set of parts where each point is connected manually with a straight line in the sketch, a volumetric comparison can be done. The results of Table 2 indicate that there is little variation between the straight line and spline curve methods of connecting the individual probe points. It also useful to analyze the volumetric change in the development of the CAD models as the height profiles progress from 3 to 5 to 10 points:

Table 2: Volumetric Comparison of CAD Parts Using Straight Line and Spline Curve Connection

Part	Volume (mm3)	% Difference
3pt Spline	8024	2.95
3pt Straight	8264	
5pt Spline	7730	1.58
5pt Straight	7853	
10pt Spline	7737	0.15
10pt Straight	7749	

The results of Table 3 indicate that the largest change in volume for both the straight line and spline curve connection parts occurs when going from the 3pt to the 5pt profile. Furthermore, the percent change in volume in both the straight line and spline curve connection parts is negligible which indicates that the 10pt probing method is an acceptable limit for the number of probe points needed to determine the height profile of the part.

Table 3: Volumetric Comparison of Spline Curve Connection and Straight Line Connection Profile Development

Part	Volume (mm3)	Comparison	% Difference
3pt Spline	8024	3pt and 5pt Spline	3.73
5pt Spline	8264	5pt and 10pt Spline	0.09
10pt Spline	7730		
3pt Straight	7853	3pt and 5pt Straight	5.1
5pt Straight	7737	5pt and 10pt Straight	1.33
10pt Straight	7749		

5.4 Geometric Surface Approximations

The geometric approximations for the part surface can be overlaid with the height profile generated from the higher fidelity to make some qualitative assessments of each approximation's advantages and disadvantages. In Figure 31 below, the triangular approximation can be seen in red, overlaid with the higher fidelity height profile in black.

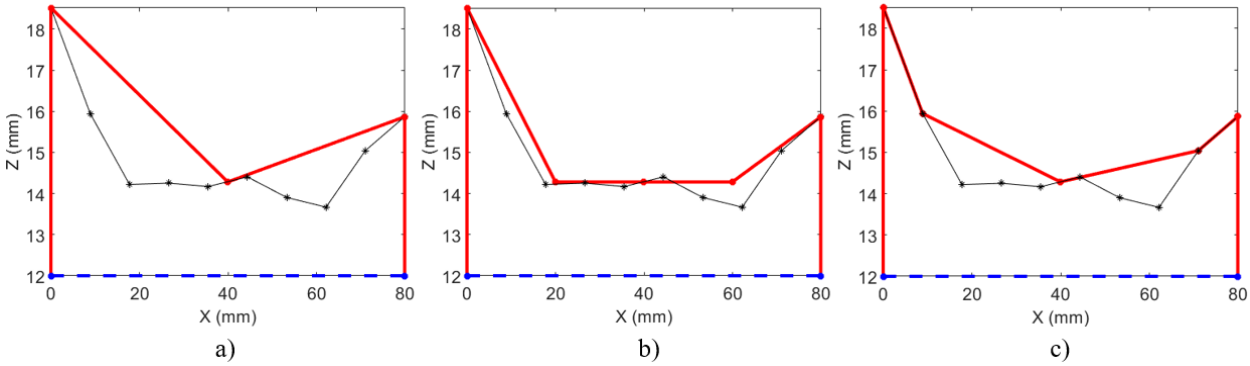

Figure 31: a) Sample Part Triangular Approximation, b) Sample Part Trapezoidal Approximation, c) Sample Part Augmented Approximation. Height profile is shown in red, desired Z height is shown by the dotted blue line, and higher fidelity height profile is shown in black.

From Figure 31a, it can be seen that the geometry produced from the triangular approximation is fairly dilated when compared to the higher fidelity height profile. This means that there is a higher safety margin for protecting the tool from crashing into peaks

in the actual height profile of the part that are not detected by the probing operation. However, this means that the tool spends more time air cutting the dilated geometry which increases the machining time. The trapezoidal approximation shown in Figure 31b has complementary advantages disadvantages to the triangular approximation. The horizontal base of the trapezoidal approximation increases the risk that an undetected peak in the actual height profile of the part causes a tool crash since the tool is traveling at rapid traverse rates. Consequently, the increase portion of the toolpaths that has the tool traveling at rapid traverse rates contributes to a lower machining time. The augmented approximation is seen in Figure 31c and does a good job of compromising between the triangular and trapezoidal approximations. The triangular bottom portion of the augmented approximation allows for the increased safety of dilated geometry yet the sections of the approximation that conform to the higher fidelity height profile reduced the toolpath sections where the tool is traveling at a cutting feed rate and thus can decrease machining time.

5.5 Toolpath Optimization

To properly evaluate the optimization results, they must be compared to the non-optimized cutting condition which uses the same feed rate and axial depth of cut. The non-optimized subtractive toolpath is shown below in Figure 32a. For more clarity, the range of the figure in Z has been truncated to show the part's height profile above the desired Z height. Additionally, there is separation of the toolpath segments into cutting and rapid feed rate sections. The optimized toolpaths for each approximation are projected onto the higher fidelity height profile of the part, shown in red, as seen below in Figure 32. The black circles indicate positions where the toolpath intersects the height profile.

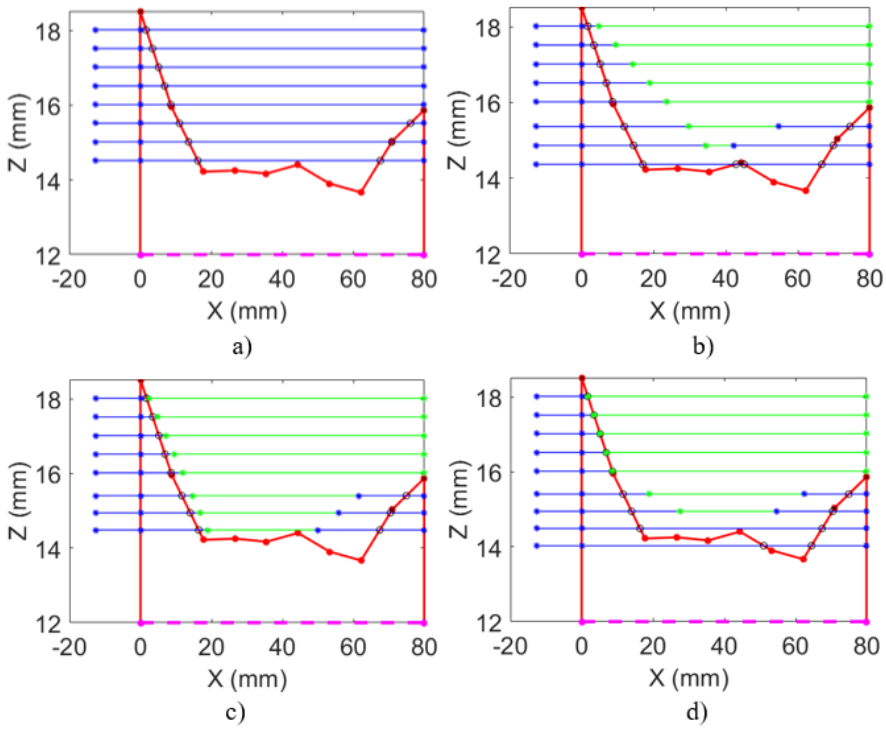

Figure 32: a) Non-optimized Subtractive Toolpath, b) Triangular Approximation Projected Optimized Toolpath, c) Trapezoidal Approximation Projected Optimized Toolpath, d) Augmented Approximation Projected Optimized Toolpath. Height profile is shown in red, desired Z height is shown by the dotted pink line. Cut feed segments are indicated by blue lines and rapid feed segments are indicated by green lines.

From Figure 32b, it can be seen that the optimized toolpath of the triangular approximation has produced the most dilated geometry and has indeed provided a higher safety margin for protecting the tool from crashing into peaks in the actual height profile. Figure 32c shows that there is a significant portion of the toolpath segments that are rapid feed rate sections which indicates a faster overall machining time. However, there is also little protection against any undetected peaks in the height profile. Lastly, the optimized toolpath using the augmented approximation, shown in Figure 32d, shows how it conforms well to the higher fidelity height profile of the part at the start and stop points of the part but provides a more dilated geometry for the middle of the part. This is beneficial as it can

contribute to a decreased machining time while reducing the risk of crashing that is inherent in the minimal probe point operations.

Table 4: Comparison of Non-Optimized and Optimized Objective Values

Objective	Non-Optimized	Triangular	Trapezoidal	Augmented
Machining Time (min)	1.9491	1.3356	1.0657	1.0868
Cutting Force*	218	92.56	74.06	83.26
Surface Roughness*	0.0317	0.0164	0.0117	0.0132

The numerical comparison of the non-optimized and optimized objective values can be found in Table 4, where objective values for cutting force and surface roughness are determined by equations (9) and (12), respectively. The table shows that for each optimization, the objective values are lower than those of the non-optimized cutting condition. It should also be noted that the trapezoidal approximation had the lowest objective values with the least dilated geometry, while the triangular approximation had the highest objective values and the most dilated geometry. The augmented approximation had objective values that were between the trapezoidal and the triangular and had dilated geometry toward the base of the part but conformed well to the start and stop points of the part's height profile. This illustrates that achievement in decreasing objective values comes at a cost of increased risk of crashing a tool.

5.6 Multi-Objective Prioritization

The previous section focused on optimization results where each optimization objective is prioritized equally, meaning that in the objective function all of the weights Wt, Wr, and Wf, are the same value. However, this is seldom the case in an actual production

environment. Depending on the component produced, the material being used, or the production schedule, different optimization objectives may need to be prioritized above others. To understand the relationship between prioritization of optimization objectives and different geometric approximations used, it is beneficial to run several test scenarios where each optimization objective is highly prioritized above the others. To establish prioritization of different objectives, the weight of the prioritized objective is set 0.8, and the other two weights are set at 0.1 so that all weights still add to 1. While the actual values from these optimization studies can be found in Appendix A, a more insightful approach is to compare the outcomes in terms of their percent change from the non-optimized cutting condition, which can be found in Tables 5-8 below.

Table 5: Machining Time Objective Prioritization

Geometric Approximation	% Change from Non-Optimized Machining Time	% Change from Non-Optimized Surface Roughness	% Change from Non-Optimized Cutting Force	Adaptive Layer Thickness (mm)	Adaptive Feed Rate (mm/min)
Triangular	-57.3556	+21.76	-0.13	0.41	531
Trapezoidal	-69.4479	+5.67	-2.75	0.46	461
Augmented	-68.56	+8.2	-0.615	0.46	471

Table 6: Cutting Force Objective Prioritization

Geometric Approximation	% Change from Non-Optimized Machining Time	% Change from Non-Optimized Surface Roughness	% Change from Non-Optimized Cutting Force	Adaptive Layer Thickness (mm)	Adaptive Feed Rate (mm/min)
Triangular	-1.664	-68.77	-74.4	0.41	136
Trapezoidal	-3.8643	-82.64	-83.96	0.46	76
Augmented	-0.58	-80.12	-81.85	0.46	86

It can be seen from Tables 5 and 6 that for all geometric approximations, the objective prioritization cases did not result in substantial decreases in the objective values. In the cases where machining time is prioritized, the cutting force objective is decreased only very slightly whereas the surface roughness objective is actually increased. In the cases where the cutting force objective is prioritized, there is a substantial decrease in the cutting force and surface roughness but only a small decrease in the machining time. While these drawbacks may be acceptable in certain production environments for certain parts, it can be assumed that an ideal optimization would have substantial decreases in all objective values.

Table 7: Surface Roughness Objective Prioritization

Geometric Approximation	% Change from Non-Optimized Machining Time	% Change from Non-Optimized Surface Roughness	% Change from Non-Optimized Cutting Force	Adaptive Layer Thickness (mm)	Adaptive Feed Rate (mm/min)
Triangular	-21.7894	-57.41	-65	0.41	186
Trapezoidal	-40.066	-67.5	-70.25	0.46	141
Augmented	-36.39	-65.3	-68.16	0.46	151

Table 8: Equal Objective Prioritization

Geometric Approximation	% Change from Non-Optimized Machining Time	% Change from Non-Optimized Surface Roughness	% Change from Non-Optimized Cutting Force	Adaptive Layer Thickness (mm)	Adaptive Feed Rate (mm/min)
Triangular	-31.4781	-48.2	-57.49	0.41	226
Trapezoidal	-45.3242	-63.1	-66.03	0.46	161
Augmented	-44	-58.36	-61.8	0.46	181

By looking strictly at the numerical values of the percent changes in the remaining objective prioritization scenarios of surface roughness and equal prioritization, it would

appear that the trapezoidal approximation would be the ideal one since it has the highest percent decreases. However, the trapezoidal approximation is also the one that is at most risk for crashing the tool into unexpected peaks in the part's height profile. If the wire DED process is not well understood and the outcome of the deposition is not well controlled, the risk of crashing could be even higher. The augmented approximation has percent decreases in the equal prioritization and surface roughness prioritization scenarios that are lower than those of the trapezoidal approximation, but only by a few percentage points. Additionally, the augmented approximation has the added benefit of being less susceptible to undetected peaks in the height profile.

5.7 Total Optimization Process Time

Up to this point, the probing operation process time has not yet been taken into account when considering the overall optimization process time. While the probe process uses minimal points that probing time must be accounted for when comparing the optimization process to the non-optimized toolpath. As such, Figure 33 below shows a comparison of the non-optimized machining time to the different total optimization process times using the augmented geometric approximation for each of the four objective prioritization scenarios.

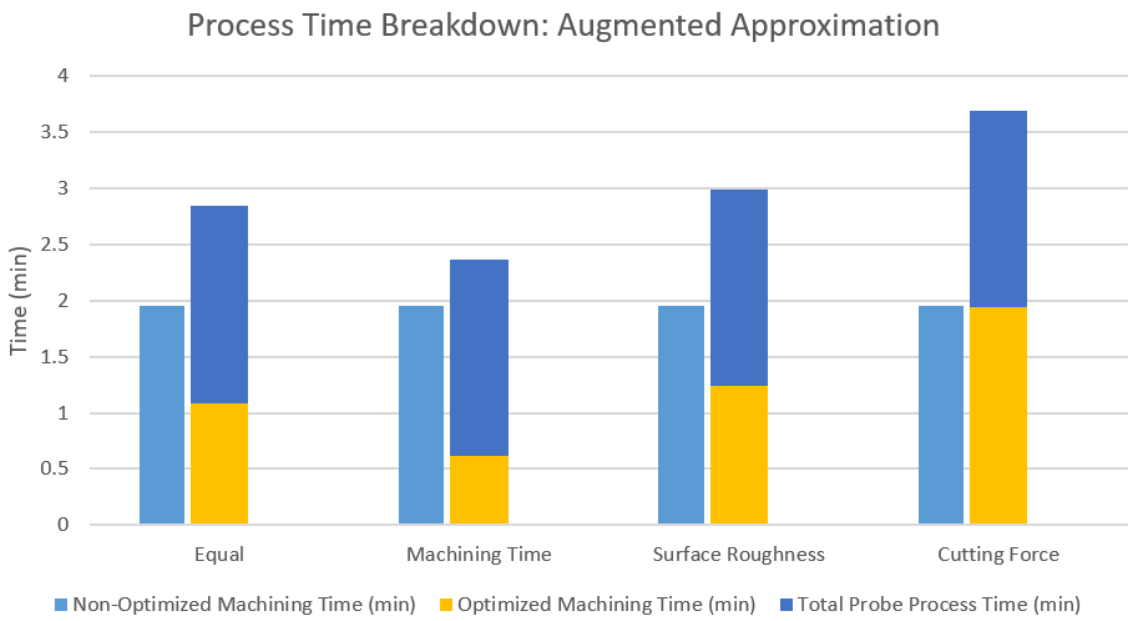

Figure 33: Process Time Breakdown Original

It can be seen that the total optimization process time exceeds the non-optimized process time for each of the four objective prioritization scenarios. While this ratio may change depending on the length of part being probed and machined, it also important to note that this comparison is for a part that is three beads wide and is assumed to be machined using a single facing pass per layer. Therefore, it is desirable to determine the effect of the number of bead being probed per part and the number of facing passes being taken per layer.

Figure 34a shows that when the number of beads is reduced to one, the total optimization process time is lower than the non-optimized process time for every objective prioritization scenario except the cutting force prioritization. Figure 34b shows that when the number of facing passes is increased to two, the total optimization process time is lower than the non-optimized process time for every objective prioritization scenario. This serves as a guidance on how to select which hybrid machine tool, in terms of its bead width

capability, to use for certain parts. It also can be inferred from Figure 37 that this optimization process is most useful for parts constructed of fewer, thicker beads as that drastically reduces the probing time and thus the overall optimization process time.

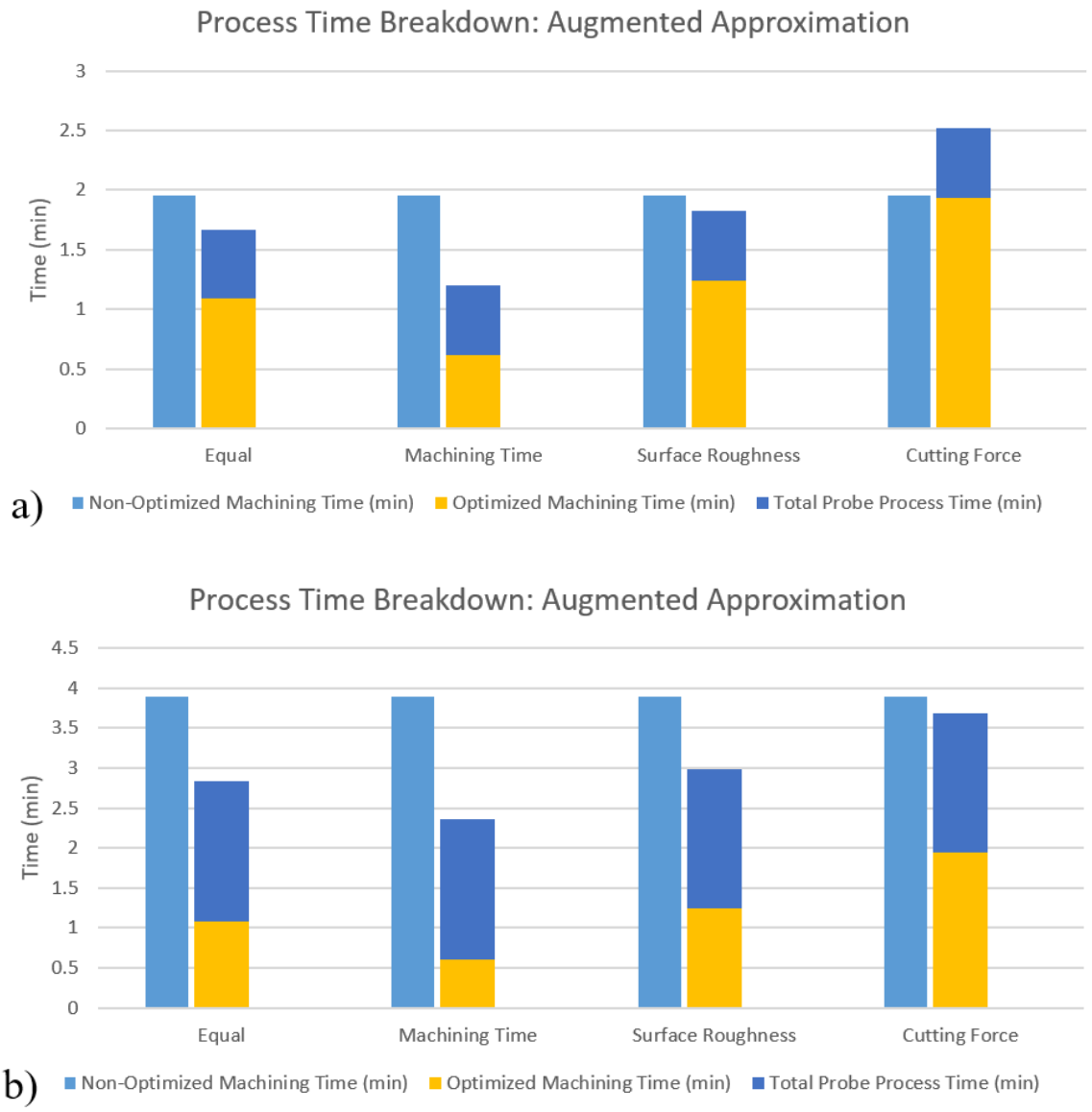

Figure 34: a) Process Time Breakdown with 1 bead and 1 Facing Pass, b) Process Time Breakdown for 3 beads and 2 Facing Passes

CONCLUSIONS AND RECOMMENDATIONS

6.1 Original Contributions

A low-cost digital architecture was implemented with the ability to transmit touch probe wirelessly using MTConnect and without the need for a permanent LAN-connected laptop. A method for easily modifying a standard touch probe command was demonstrated for use in generating 3-axis probe toolpaths designed to probe part surfaces. The geometric surface approximation of wire-based DED parts had not been previously studied and the restriction of using minimal probe points to form those geometric surface approximations represents a novel and efficient method for approximating part surface geometry. Subtractive manufacturing toolpath optimization studies had not been applied to the unique challenges inherent in performing a 3-axis facing operation on an irregular part surface geometry so this work provides some insight into how to adapt and optimize machining toolpaths for use in hybrid machine tools that produce irregular part surfaces during deposition.

6.2 Conclusions

In this work a multi-objective optimization strategy for facing the surfaces of wire-based DED parts is presented. Geometric gathered about wire-based DED part surfaces via an on-machine touch probe is used to construct a digital twin using different geometric surface approximations: triangular, trapezoidal and augmented. Different optimization scenarios are then conducted using the different geometric surface approximations and

prioritizing the different optimization objectives of minimizing machining time, cutting force, and surface roughness so that the effect on the optimization goals could be evaluated.

The multi-objective optimization results for all prioritization scenarios also show that the triangular approximation performed the worst in terms of percent changes in optimization goals from the non-optimized cutting condition and the trapezoidal approximation performed the best in terms of percent changes in optimization goals from the non-optimized cutting condition. The optimization results for the augmented approximation show that while it did not perform as well as the trapezoidal approximation, the percent changes are very close to those of the trapezoidal approximation with the largest discrepancy between the results of the augmented and trapezoidal approximations being approximately five percentage points. An analysis of the different optimization prioritization scenarios concludes that the prioritization scenarios where machining time and cutting force are prioritized result in poor improvements in the other two optimization objectives, with the machining time prioritization actually resulting in an increase in surface roughness for all geometric surface approximations. While some production scenarios may wish to prioritize machining time or cutting force, it is important to realize the performance trade-offs in the other optimization objectives. An important qualitative factor in comparing the toolpaths generated by these geometric approximations is the risk of crashing the tool in to the part surface when traveling at a rapid feed rate. The toolpath created by the triangular approximation has a low risk of the tool crashing into the part during the rapid feed rate toolpath segments since the surface geometry created by the triangular approximation is mostly above the actual part surface geometry. The toolpath created by the trapezoidal approximation has a high risk of crashing during these rapid feed

rate segments since the middle section of the surface geometry created by the trapezoidal approximation (the base of the trapezoid) is mostly at the same height as the actual part surface geometry. Like the triangular approximation, the toolpath created by the augmented geometric surface approximation provides a low risk of crashing the tool during the rapid feed rate segments. Therefore, the augmented approximation is the best approximation option as the toolpath generated provides a low risk of crashing the tool and provides improvements in machining time, surface roughness and cutting force that are comparable to those of the trapezoidal approximation.

When the overall optimization process time, meaning the combined process times of probing and optimized machining, is compared to the non-optimized process time for different numbers of facing passes and beads per part it is shown that the optimized process time becomes substantially lower than the non-optimized process time when the number of beads per part is decreased and when the machining operation is conducted with multiple facing passes. This means that this optimization process is well suited for parts constructed of a few thick beads rather than many thinner ones.

6.3 Future Work Recommendations

The methods described and performed in this work were done piecemeal and did not have a software package that incorporated all of them together. For future areas of study, it would be beneficial to the apply optimization algorithm and probe toolpath generation to existing CAM software like Fusion360 or rewrite and combine those algorithms in open source software like Python. Additionally, it would be beneficial to incorporate statistical data about the variations in the weld geometry to the geometric surface approximations so

that a proper assessment of crashing risk can be conducted. Lastly, the multi-objective approach only utilized three competing objectives when in reality there are a wide variety of possible additions like total energy consumption and vibration analysis for thin-walled structures.

APPENDIX A. OPTIMIZATION PRIORITIZATION STUDY VALUES

A.1 Triangular Approximation

Objective Prioritized	Machining Time (min)	Surface Roughness	Cutting Force	Adaptive Layer Thickness (mm)	Adaptive Feed Rate (mm/min)
Equal Weight	1.3356	0.0164	92.66	0.41	226
Machining Time	0.8312	0.0386	217.71	0.41	531
Surface Roughness	1.5244	0.0135	76.26	0.41	186
Cutting Force	1.9167	0.0099	55.76	0.41	136

A.2 Trapezoidal Approximation

Objective Prioritized	Machining Time (min)	Surface Roughness	Cutting Force	Adaptive Layer Thickness (mm)	Adaptive Feed Rate (mm/min)
Equal Weight	1.0657	0.0117	74.06	0.46	161
Machining Time	0.5955	0.0335	212	0.46	461
Surface Roughness	1.1682	0.0103	64.86	0.46	141
Cutting Force	1.8738	0.0055	34.96	0.46	76

A.3 Augmented Approximation

Objective Prioritized	Machining Time (min)	Surface Roughness	Cutting Force	Adaptive Layer Thickness (mm)	Adaptive Feed Rate (mm/min)
Equal Weight	1.0868	0.0132	83.26	0.46	181
Machining Time	0.6124	0.0343	216.66	0.46	471
Surface Roughness	1.2398	0.0110	69.4	0.46	151
Cutting Force	1.9378	0.0063	39.56	0.46	86

REFERENCES

[1] K. A. Lorenz, J.B. Jones, D. I Wimpenny and M.R. Jackson. “A review of hybrid manufacturing”, 2015.

[2] J. Jones, P. McNutt, R. Tosi, C. Perry and D. Wimpenny. “Remanufacture of turbine blades by laser cladding, machining and in-process scanning in a single machine”, 2012.

[3] X. Zhang, W. Cui, W. Li, F. Liou. “Metallic Components Repair Strategies Using the Hybrid Manufacturing Process,” 2017.

[4] M. Cortina et al. “Latest Developments in Industrial Hybrid Machine Tools that Combine Additive and Subtractive Operations,” Materials, Volume 11. 2018

[5] J. Nagel and F. Liou. “Hybrid Manufacturing System Design and Development,” Manufacturing System, Chapter 11. 2012.

[6] F. W. Liou et al. “Applications of a Hybrid Manufacturing Process for Fabrication of Metallic Structures,” Rapid Prototyping Journal, Volume 13. 2007.

[7] Xu et al. “Realisation of a multi-sensor framework for process monitoring of the wire arc additive manufacturing in producing Ti-6Al-4V parts,” International Journal of Computer Integrated Manufacturing, vol. 31, no. 8, pp. 785-798.

[8] Jasco et al. “The fast constant engagement offsetting method for generating milling toolpaths,” International Journal of Advanced Manufacturing Technology, Volume 103, pp 4293-4305, 2019.

[9] Uddin et al. “Constant Engagement Tool Path Generation to Enhance Machining Accuracy in End Milling,” JSME International Journal, Volume 49, Issue 1, pp 43-49, 2006.

[10] Agic et al. “Analysis of entry phase in intermittent machining,” University West, 2018.

[11] S. Liu, et al. “Real-time monitoring of laser hot-wire cladding of Inconel 625,” Opt. Lasers Technol., 62 (10) (2014), pp. 124-134

[12] Heralic et al. “Height control of laser metal-wire deposition based on iterative learning control and 3D scanning,” Opt. Lasers Eng., 50 (9) (2012), pp. 1230-1241

[13] Praniewicz et al. “Adaptive geometry transformation and repair for hybrid manufacturing,” 46th SME NAMRC, Texas, USA 2018.

[14] Kim et al. “Adaptive repair and digitization for hybrid manufacturing,” 47th SME NAMRC, Erie, Pennsylvania, USA 2019.

[15] Castelino et al. “Toolpath optimization for minimizing airtime during machining,” Journal of Manufacturing Systems, Volume 22, Issue 3, pp 173-180. 2003.

[16] Lazoglu et al. “Tool path optimization for free form surface machining,” CIRP Annals, Volume 58, Issue 1, pp 101-104. 2009.

[17] Corso et al. “Using optimization procedures to minimize machining time while maintaining surface quality,” International Journal of Advanced Manufacturing Technology, Volume 65, pp 1659 – 1667. 2013.

[18] Maiyar et al. “Optimization of Machining Parameters for End Milling of Inconel 718 Super Alloy Using Taguchi Based Grey Relational Analysis,” International Conference on Design and Manufacturing, 2013.

[19] Shaik et al. “Optimal selection of operating parameters in end milling of Al-6061 work materials using multi-objective approach,” Mechanics of Advanced Materials and Modern Processes, 2017.

[20] An et al. “Multi-Objective Optimization for Milling Operations using Genetic Algorithms under Various Constraints,” International Journal of Networked and Distributed Computing, Volume 2, pp 108-114, 2014.

[21] Ali et al. “Multi-Response Optimization of Face Milling Performance Considering Toolpath Strategies in Machining of Al-2024,” Materials, 2019.

[22] Yan et al. “Multi-objective optimization of milling parameters – the trade-offs between energy, production rate, and cutting quality,” Journal of Cleaner Production, Volume 52, pp 462-471, 2013.

[23] Sandvik Coromant. *Face Milling.* https://www.sandvik.coromant.com/en-us/knowledge/milling/pages/face-milling.aspx

[24] Gessner et al. “Computer-aided alignment of castings and machining optimization,” Journal of Mechanical Engineering Science, Volume 229, Issue 3, pp. 485-492. 2015.

[25] Mazak VC-500A/5X HWD. https://www.mazakusa.com/machines/vc-500a-5x-am-hwd/

[26] Mazak VC-500A/5X Cover Sheet, Northwest Machine Technologies, 2017.

[27] *Renishaw GoProbe Cycles for Inspection Plus: Fanuc and Meldas Controls.* Renishaw Programming Manual H-2000-6754-00-A

[28] M. Parto et al. “An MTConnect-Compatible Platform For Secured Machine Monitoring Through Integration Of Fog Computing, Cloud Computing, And Communication Protocols,” International Symposium on Flexible Automation, 2018.

[29] Nguyen et al. “Manufacturing Process Monitoring and Control in Industry 4.0,” Proceedings of 5th International Conference on the Industry 4.0 Model for Advanced Manufacturing, 2020.

[30] Liang et al. “Analysis of Machine Tools,” Springer, ISBN 978-1-4899-7643-7, 2016.

[31] S. Kalpakjian et al. “Manufacturing Processes for Engineering Materials,” Prentice Hall, NJ, ISBN 0-13-227271-7, 2008.

[32] S.S. Rao et al. “Engineering Optimization: Theory and Practice, 4th Edition,” John Wiley & Sons Inc, NJ, ISBN 978-0-470-18352-6.